

University of Windsor

Scholarship at UWindor

Electronic Theses and Dissertations

Theses, Dissertations, and Major Papers

1981

A study of the electric quadrupole interaction at hafnium-sites in antiferroelectric lead hafnate by the method of perturbed angular correlations in tantalum-181.

Mridula. Sah
University of Windsor

Follow this and additional works at: <https://scholar.uwindsor.ca/etd>

Recommended Citation

Sah, Mridula., "A study of the electric quadrupole interaction at hafnium-sites in antiferroelectric lead hafnate by the method of perturbed angular correlations in tantalum-181." (1981). *Electronic Theses and Dissertations*. 797.

<https://scholar.uwindsor.ca/etd/797>

This online database contains the full-text of PhD dissertations and Masters' theses of University of Windsor students from 1954 forward. These documents are made available for personal study and research purposes only, in accordance with the Canadian Copyright Act and the Creative Commons license—CC BY-NC-ND (Attribution, Non-Commercial, No Derivative Works). Under this license, works must always be attributed to the copyright holder (original author), cannot be used for any commercial purposes, and may not be altered. Any other use would require the permission of the copyright holder. Students may inquire about withdrawing their dissertation and/or thesis from this database. For additional inquiries, please contact the repository administrator via email (scholarship@uwindsor.ca) or by telephone at 519-253-3000ext. 3208.



National Library of Canada
Collections Development Branch

Canadian Theses on
Microfiche Service

Bibliothèque nationale du Canada
Direction du développement des collections

Service des thèses canadiennes
sur microfiche

NOTICE

The quality of this microfiche is heavily dependent upon the quality of the original thesis submitted for microfilming. Every effort has been made to ensure the highest quality of reproduction possible.

If pages are missing, contact the university which granted the degree.

Some pages may have indistinct print especially if the original pages were typed with a poor typewriter ribbon or if the university sent us a poor photocopy.

Previously copyrighted materials (journal articles, published tests, etc.) are not filmed.

Reproduction in full or in part of this film is governed by the Canadian Copyright Act, R.S.C. 1970, c. C-30. Please read the authorization forms which accompany this thesis.

**THIS DISSERTATION
HAS BEEN MICROFILMED
EXACTLY AS RECEIVED**

AVIS

La qualité de cette microfiche dépend grandement de la qualité de la thèse soumise au microfilmage. Nous avons tout fait pour assurer une qualité supérieure de reproduction.

S'il manque des pages, veuillez communiquer avec l'université qui a conféré le grade.

La qualité d'impression de certaines pages peut laisser à désirer, surtout si les pages originales ont été dactylographiées à l'aide d'un ruban usé ou si l'université nous a fait parvenir une photocopie de mauvaise qualité.

Les documents qui font déjà l'objet d'un droit d'auteur (articles de revue, examens publiés, etc.) ne sont pas microfilmés.

La reproduction, même partielle, de ce microfilm est soumise à la Loi canadienne sur le droit d'auteur, SRC 1970, c. C-30. Veuillez prendre connaissance des formules d'autorisation qui accompagnent cette thèse.

**LA THÈSE A ÉTÉ
MICROFILMÉE TELLE QUE
NOUS L'AVONS REÇUE**

A STUDY OF THE ELECTRIC QUADRUPOLE INTERACTION AT
Hf-SITES IN ANTIFERROELECTRIC LEAD HAFNATE BY THE
METHOD OF PERTURBED ANGULAR CORRELATIONS IN ^{181}Ta



by
Mridula Sah

A Thesis

Submitted to the Faculty
of Graduate Studies through the
Department of Physics in Partial Fulfillment
of the Requirements for the Degree of Master of Science
at the University of Windsor

Windsor, Ontario, Canada

1981

ABSTRACT

The static electric quadrupole interaction in polycrystalline and single crystalline PbHfO_3 at Hf-sites has been investigated by the perturbed angular correlation method.

The quadrupole interaction frequency w_Q , the electric field gradient V_{zz} , the asymmetry parameter η , the smearing δ were determined as a function of temperature. The direction of the field gradient was established by determining the polar angle β and the azimuthal angle α defined with respect to a coordinate system whose z-axis is the c-axis. The variation of the direction of V_{zz} with temperature was also studied. The frequencies were also determined by the numerical integration of the perturbed function over a finite time interval $T = 36$ ns.

The investigations confirm the structural phase transformations undergone by the antiferro-electric PbHfO_3 .

DEDICATION

I dedicate this thesis to my parents.

ACKNOWLEDGEMENTS

I would like to thank all those who have helped me to complete this work. My special thanks go to Dr. E.E.Habib my research Supervisor; Dr. H. Ogata for his patience and help during the preparations for this thesis and for his help in the theoretical calculations.

I am also indebted to the University of Windsor for their financial support in the form of Scholarships.

LIST OF TABLES

	Page
I Time Calibration	61
II Experimental Results for Polycrystalline Source	62
III-VII Experimental Results for Single Crystal source	63
VIII Values of various parameters for polycrystalline source	87
IX Variation of parameters with temperature for single crystal source	88
X Variation of w_Q and $ V_{ZZ} $ with temperature	89

LIST OF FIGURES

	Page	
2.1.1	Two nuclear radiations emitted in cascade and the quantum numbers involved	6
2.3.1	Precession of the nuclear angular momentum I and the electric quadrupole moment Q around any symmetry axis	12
2.4.1	Angular co-ordinates of propogation directions k_1 and k_2	17
2.5.1	Position of z' axis defined by Euler angles	22
3.1.1	Simple coincidence circuit	41
3.3.1	Block diagram of apparatus	47
3.4.1	^{181}Hf decay scheme	50
3.4.2	^{60}Co decay scheme	53
3.4.3	^{60}Co coincidence Spectrum	54
3.5.1	Single Crystal PbHfO_3	57
3.5.2	Detector geometry	58
4.1.1	Anisotropy vs time for polycrystalline source	68
4.1.2-6	Anisotropy vs time for single crystal source at various temperatures	69
4.2.1-6	Power spectra for perturbation functions	79
4.2.7	Geometry of Apparatus showing Euler angles	85
4.2.8	PbHfO_3 crystalline structure	86

TABLE OF CONTENTS

	Page
ABSTRACT	iii
DEDICATION	iv
ACKNOWLEDGEMENTS	v
LIST OF TABLES	vi
LIST OF FIGURES	vii
Chapter I : Introduction	1
Chapter II : Theory of Angular Correlation	4
2.1 Introduction	4
2.2 Unperturbed Angular Correlation	7
2.3 Perturbed Angular Correlation: Influence of Extranuclear Fields	9
2.4 Mathematical treatment of Extranuclear Perturbations	14
2.5 Static Interactions (Classical Fields)	20
2.6 Static Electric Quadrupole Interaction	28
2.7 Adaption of Theoretical Results for Experiment	
(a) Theoretical Results	36
(b) Experimental Formulae	38
Chapter III : Experiment	
3.1 Introduction	40
3.2 Experimental Correlation Function	42
3.3 Apparatus	46
3.4 Working of the Apparatus	48

Contents contd.

	Page
Chapter III : 3.5 Experimental Procedure	55
Chapter IV : Results and Discussion	
4.1 Results	59
4.2 Discussion of Results	74
Appendix :	90
Bibliography	102
Vita Auctoris	103

CHAPTER I

INTRODUCTION

The study of the interaction of the atomic nucleus with extranuclear fields has proven quite useful in many contexts. Nuclear resonance and spectroscopic techniques have, for example been valuable in elucidating the nature of chemical bonding in molecules and compounds and in characterizing the properties of magnetic materials. In non-magnetic substances, the nuclear electric quadrupole interaction (QI) has had wide applicability as an aid to determining the distribution of electric charge surrounding a nuclear site. The experimental techniques most commonly used for this purpose are nuclear magnetic and quadrupole resonance, Mossbauer effect and perturbed angular correlations. The former two are appropriate for measurements on the stable nuclear ground states of relatively abundant species in the sample under consideration. Perturbed angular correlation methods are good for measurements of the quadrupole interactions with dilute concentrations of impurity ions.

This method has been shown to be a useful tool for the study of hyperfine interactions in solids. This provides information about the strength and symmetry of the electric field gradient (EFG) at the nuclear site, and as such has been used in studies

of high co-ordination complexes, which surround the differential perturbed angular correlation (DPAC) probe nucleus. An advantage of DPAC when compared to the Mossbauer effect is that it can be used over a wide range of temperature and thus is specially useful to detect temperature dependent conformational interconversions that might occur in these compounds.

Compounds possessing perovskite - type structure are usually ferro-electric or anti-ferroelectric. A study of the internal electric field gradient in these compounds is of great interest. The reason is that since the EFG reflects the microscopic charge distribution, its determination and especially the investigation of its temperature dependence should contribute to the collective phenomena in ferro-electric and anti-ferroelectric substances.

A possibility of using nuclei as a microscopic field sensitive probe is due to the fact that the angular correlation of two successive gamma-rays can be perturbed by the hyperfine interaction between the nuclear moments of the intermediate state of the cascade and the electromagnetic field acting on the nucleus. In particular, the electric quadrupole interaction with the EFG can be measured provided the nuclear spin is greater than or equal to unity.

This thesis presents a study of the temperature

dependence of the EFG and the quadrupole frequency in anti-ferroelectric lead hafnate (PbHfO_3) by the method of time differential perturbed angular correlation (TDPAC). The variation of the direction of the EFG with temperature is also studied.

These experiments at various temperatures were conducted in order to investigate the series of structural phase transformations which the perovskite compound PbHfO_3 undergoes. (P.D. Dernier et al. 1975). The change in the structure influences the crystalline field and hence the magnitude and direction of the electric field gradient. Therefore, these experiments were designed to investigate the temperature dependence of the quadrupole perturbation interaction, i.e. the effect of temperature on anisotropy.

CHAPTER II

THEORY OF ANGULAR CORRELATION

2.1 Introduction:

Angular correlation can be defined as follows: a nucleus decays from an initial level by emitting radiation R_1 in the direction \vec{k}_1 , to an intermediate level and from there through the emission of radiation R_2 in the direction \vec{k}_2 to the final state. Since the nuclei (and hence nuclear spins) are randomly oriented, the intensity distribution of the first radiation R_1 will be isotropic.

Now, consider an arbitrary axis constructed through the source along which the first radiation is detected. This causes the magnetic sub-levels, m , of the intermediate level to be populated according to the transition probabilities $m_i \rightarrow m$. Thus, such an observation gives rise to an ensemble of nuclei with an unequal population of magnetic sub-levels. Because of these unequal populations the radiation R_2 corresponding to the sum of all transition probabilities $m \rightarrow m_f$, then has a definite anisotropic distribution with respect to the direction \vec{k}_1 of the first radiation. (Fig. 2.1.1). The intensity distribution of the second radiation with respect to the direction of the first radiation is known as the angular correlation of the two nuclear radiations.

Mathematically, the angular correlation described above can be defined in terms of the "correlation function" $W(\theta)dw$, where $W(\theta)dw$ is the relative probability that radiation R_2 is emitted at an angle θ with respect to the direction \vec{k}_1 of the first radiation R_1 into the solid angle dw .

When the nucleus is not disturbed by extranuclear fields and the unequal m -population in the intermediate level is preserved until the second radiation is emitted then "unperturbed angular correlation" results. This happens when the mean life τ_b of the intermediate level is shorter than the interaction time $h/\Delta E$, where ΔE is the interaction energy between the nucleus and the extranuclear fields. For very short-lived cases ($\tau_b \ll 10^{-11}$ secs.) this condition is always satisfied. But for states with longer lifetimes, perturbations are possible, and the unequal population of the m -states in the intermediate level is changed, thus resulting in change in correlation. This is known as the "perturbed angular correlation".

Generalizations of the theory of cascade radiations and, expressing the results in the form that can be readily applied to experimental data has been worked on by many. The progress is largely due to the use of three tools: (i) group theory (ii) Racah algebra and (iii) density matrices. The mathematical preliminaries for the development of this theory is given in the Appendix.

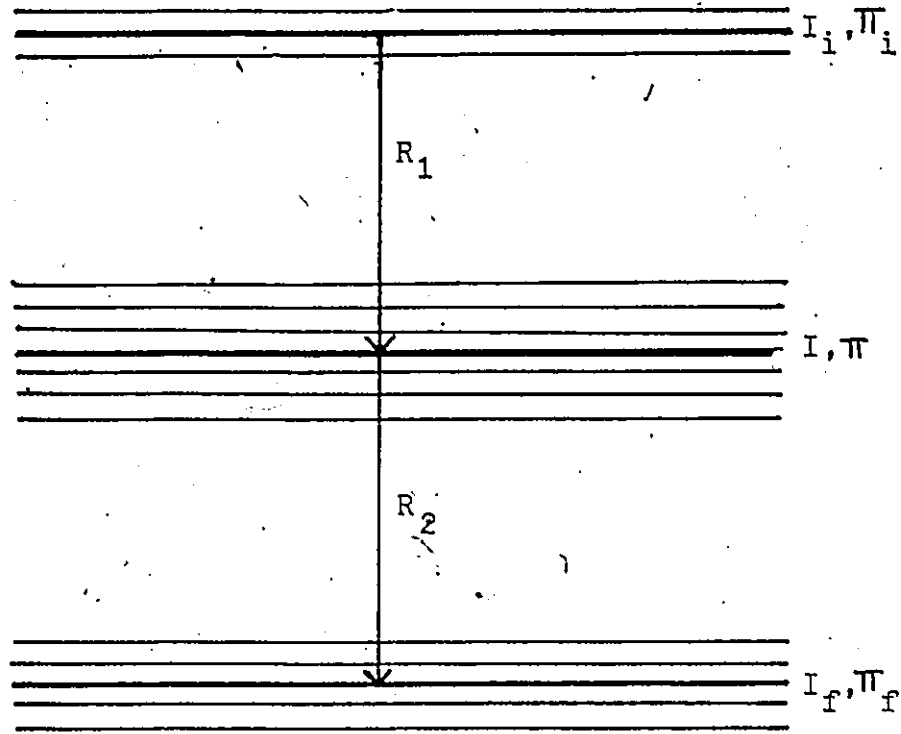


Fig. 2.1.1: Two nuclear radiations emitted in cascade and the quantum numbers involved (π_i, π, π_f represent the parities of the initial, intermediate and final states respectively).

2.2 Unperturbed Angular Correlation:

In this sub-section, the directional correlation function $W(\vec{k}_1, \vec{k}_2) d\Omega_1 d\Omega_2$ is defined as the probability that a nucleus decaying through the cascade $I_i \rightarrow I \rightarrow I_f$ emits two radiations R_1 and R_2 in the directions \vec{k}_1 and \vec{k}_2 into the solid angles $d\Omega_1$ and $d\Omega_2$. The derivation is based on the first order perturbation theory.

Consider a nucleus decaying from a randomly populated level i with spin I_i , described by the density matrix P_i to the intermediate level with spin I ; the emitted radiation R_1 is observed in the direction \vec{k}_1 . Perturbation theory in the first order describes this process and yields the density matrix for the intermediate level, P . The second step in the cascade $I \rightarrow I_f$ is treated in the same manner, differing only in that the density matrix is not known a priori, but is the result of the preceding transition.

Consider the transition $I_i \rightarrow I$. Applying Eqn. (A.31) to this transition by setting $a = m_i$ and $b = m$ and $\rho = P$, we get:

$$\langle m | P | m' \rangle = S_1 \sum_{m_i, m'_i} \langle m | H_1 | m_i \rangle \langle m_i | P_i | m'_i \rangle \times \langle m' | H_1 | m'_i \rangle^* \quad (2.2.1)$$

In the above equation and in all the following equations, angle independent factors have been assumed to be unity. The symbol S_1 indicates summation over all unmeasured radiation properties, such as spin and polarization. Using Eqn.(A.25), the Eqn. (2.2.1) becomes:

$$\langle m | P | m' \rangle = S_1 \sum_{m_i} \langle m | H_1 | m_i \rangle \langle m_i | H_1 | m' \rangle \quad (2.2.2)$$

For the second transition from the intermediate level to the final level, set $a = m$ and $b = m_f$ in Eqn.(A.31) and apply. Thus we get

$$W(\vec{k}_1, \vec{k}_2) = S_1 S_2 \sum_{m_f} \sum_{m, m'} \langle m_f | H_2 | m \rangle \langle m | P | m' \rangle \times \langle m' | H_2 | m_f \rangle \quad (2.2.3)$$

Substituting Eqn. (2.2.2) into Eqn. (2.2.3) gives:

$$W(\vec{k}_1, \vec{k}_2) = S_1 S_2 \sum_{m_f, m, m', m_i} \langle m_f | H_2 | m \rangle \langle m | H_1 | m_i \rangle \times \langle m_i | H_1 | m' \rangle \langle m' | H_2 | m_f \rangle \quad (2.2.4)$$

2.3 Perturbed Angular Correlation: Influence of Extranuclear Fields:

The angular correlation of a cascade $I_i \rightarrow I \rightarrow I_f$ will, in general be altered as soon as the nuclei in their intermediate level I are subject to torques, due to the interaction of either the magnetic dipole moment μ with an extranuclear magnetic field \vec{B} , or of the electric quadrupole moment Q with the field gradient (EFG) $\partial^2 V / \partial z^2$, i.e. V_{zz} . We will consider only the perturbation of the angular correlation due to the interaction of Q with V_{zz} .

By a proper choice of axes, using Laplace's equation and the axial symmetry of the field, the field gradient can be expressed in terms of V_{zz} only where the z -axis is chosen as the symmetry axis. The generalization to non-axial (rhombic) fields can be considered by introducing an asymmetry parameter

$$\eta = \frac{|V_{xx} - V_{yy}|}{V_{zz}}$$

Axially symmetric field gradients are assumed in the following discussions.

In a semi-classical picture, the interaction between such an electric field gradient and a nuclear electric quadrupole moment gives rise to an aligning torque exerted on the nucleus. The resulting precession of the angular momentum about the z -axis of the field gradient

has several characteristic frequencies which depend on the relative orientation of the nuclear spin axis I with respect to the axis of the field (z -axis). (See Fig. 2.3.1). This is also seen in the non-equidistant splitting of the $2I + 1$ energy levels caused by the electric quadrupole coupling.

The potential energy of such a system where the position of the axis of the quadrupole moment with respect to the field axis (z -axis) is specified by the magnetic quantum number m_z is given by:

$$E_Q(m_z) = \left[3m_z^2 - I(I+1) \right] \frac{eQV_{zz}}{4I(2I-1)} \quad (2.3.2)$$

Positions of I correspond to $+m_z$ and $-m_z$ (angle θ and $180 - \theta$) respectively and have the same energy giving rise to two-fold degeneracy. Classically, this degeneracy is explained by the vector I precessing in one direction for angle $\theta < 90^\circ$ ($+m_z$) and with the same precession frequency but in the opposite direction for the angle $180^\circ - \theta$ ($-m_z$). Thus the quadrupole precession is not unidirectional like the magnetic precession.

The characteristic frequencies correspond to the energy differences between neighbouring levels and expressed in terms of frequency w_e , where

$$w_e = \frac{\Delta E_Q}{h} = \frac{1}{h} \left[E_Q(m_z) - E_Q(m'_z) \right] \quad (2.3.3)$$

The smallest non-vanishing frequency is given by

$$\omega_e^0 = \frac{3eQV_{zz}}{4I(2I-1)h} \quad \text{for integer } I \quad (2.3.4)$$

$$\omega_e^0 = \frac{3eQV_{zz}}{2I(2I-1)h} \quad \text{for half-integer } I \quad (2.3.5)$$

The common feature of static electric interactions is the precession of the nuclear spin around a well defined stationary axis, the symmetry axis of the field. In the preceding discussion, this axis was used as the quantization axis for which the m_z values were defined. The precession of I does not change these projections i.e. the interactions do not induce transitions between the m_z sublevels, defined with respect to the field axis as the axis of quantization. But, the population of the m -sublevels defined with respect to a direction other than the field direction as the axis of quantization changes periodically with the precession of I about the field axis. This change causes an attenuation of the correlation as the second radiation is emitted from a level with altered population. In the language of density matrices, the transition among m -states are described by a time dependence in the density matrix of the intermediate state.

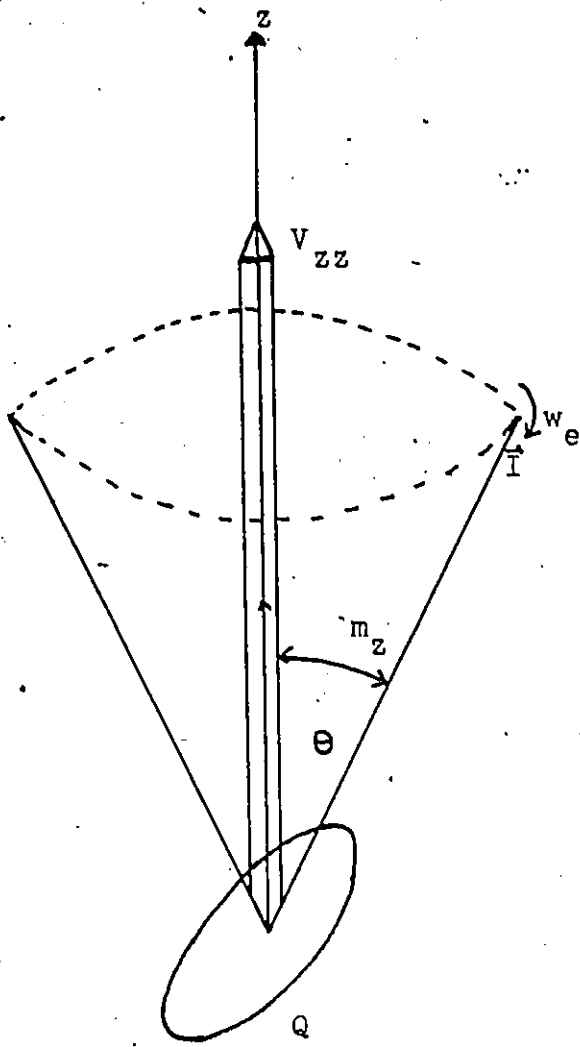


Fig. 2.3.1: The precession of the nuclear angular momentum \vec{I} and the electric quadrupole moment Q around the symmetry axis of an electrostatic gradient.

But, if the field axis z coincides with the axis representing the direction of emission of radiation \vec{k}_1 used for the introduction of unequally populated m_{k_1} states then the m_z are the same as m_{k_1} . Since m_z does not change neither does m_{k_1} and the correlation is unperturbed.

The influence of extranuclear fields on angular correlation depends on the magnitude of the interaction and the time for which it acts i.e. on the mean lifetime τ_b of the intermediate stage. Perturbed angular correlation results if $w_e \tau_b \gg 1$.

2.4 Mathematical Treatment of Extranuclear

Perturbations:

Expression 2.2.4 may be written as:

$$\begin{aligned}
 W(\vec{k}_1, \vec{k}_2, 0) = & \sum_{m_i, m_a, m_b} \sum_{m'_a, m'_b, m_f} \langle m_f | H_2 | m_b \rangle \\
 & \times \langle m_a | H_1 | m_i \rangle \delta_{m_a m_b} \\
 & \times \langle m_f | H_2 | m'_b \rangle^* \langle m'_a | H_1 | m_i \rangle^* \delta_{m'_a m'_b} \quad (2.4.1)
 \end{aligned}$$

H_1 and H_2 represent the interaction between the nucleus and the radiation field. In the absence of extranuclear perturbations the final states $\langle m_a |$ and $\langle m'_a |$ after emission of the first radiation are identical with the initial states $| m_b \rangle$ and $| m'_b \rangle$ of the second radiation. (Fig. 2.1.1).

Assume that the nucleus interacts with an extranuclear field while it is in its intermediate state. The interaction is described by the Hamiltonian K and is assumed to act from the time of emission of the first radiation ($t=0$) until the time t at which the second radiation is emitted.

During this time interval the states $| m_a \rangle$ change to different states $| m_b \rangle$ under the influence of extranuclear perturbation. This change can be described by a unitary operator $\lambda(t)$ that describes the evolution of the state vectors $| m_a \rangle$. Thus the

perturbed angular correlation can be expressed as:

$$\begin{aligned}
 W(\vec{k}_1, \vec{k}_2, t) = & \sum_{m_i, m_f} \sum_{m_a, m'_a} \langle m_f | H_2 \lambda(t) | m_a \rangle \\
 & \times \langle m_a | H_1 | m_i \rangle \langle m_f | H_2 \lambda(t) | m'_a \rangle^* \\
 & \times \langle m'_a | H_1 | m_i \rangle^* \quad (2.4.2)
 \end{aligned}$$

The states $|m\rangle$ form a complete set and thus the state vector $\lambda(t)|m_a\rangle$ can be expressed as:

$$\lambda(t)|m_a\rangle = \sum_{m_b} \langle m_b | \lambda(t) | m_a \rangle | m_b \rangle \quad (2.4.3)$$

Similarly

$$\lambda(t) | m'_a \rangle = \sum_{m'_b} \langle m'_b | \lambda(t) | m'_a \rangle | m'_b \rangle \quad (2.4.4)$$

The time evolution operator satisfies the Schroedinger equation:

$$\frac{\partial}{\partial t} (\lambda(t)) = -iK \frac{\lambda(t)}{\hbar} \quad (2.4.5)$$

For time dependent interaction, the solution of the Eqn. (2.4.5) is:

$$\lambda(t) = \exp \frac{-iKt}{\hbar} \quad (2.4.6)$$

The perturbed angular 'correlation function' becomes:

$$\begin{aligned}
 W(\vec{k}_1, \vec{k}_2, t) = & \sum_{m_f, m_i} \sum_{m_a, m_b} \sum_{m'_a, m'_b} \langle m_f | H_2 | m_b \rangle \\
 & \times \langle m_b | \lambda(t) | m_a \rangle \langle m_a | H_1 | m_i \rangle \\
 & \times \langle m_f | H_2 | m'_b \rangle^* \langle m'_b | \lambda(t) | m'_a \rangle^* \\
 & \times \langle m'_a | H_1 | m_i \rangle^* \qquad (2.4.7)
 \end{aligned}$$

The matrix elements $\langle m' | H_i | m \rangle$ for the emission of the i^{th} nuclear radiation are replaced by the expressions obtained by using the transformation properties, rotational matrices and Clebsch-Gordan coefficients. When the summation over m_i and m_f are performed and the correlation restricted to directional correlation only, the matrix elements become:

$$\begin{aligned}
 \sum_{m_i} \langle m_a | H_1 | m_i \rangle \langle m'_a | H_1 | m_i \rangle^* = & \sum_{L, L'} \sum_{k, N} (-1)^{2I - I_i + m - L'} \\
 & \times (2k_1 + 1)^{\frac{1}{2}} \begin{pmatrix} I & I & k_1 \\ m'_a & -m_a & N_1 \end{pmatrix} \begin{Bmatrix} I & I & k_1 \\ L & L' & I_i \end{Bmatrix} \times C_{k_0}(L, L') \\
 & \times \langle I || L, \pi || I_i \rangle \langle I || L', \pi' || I_i \rangle^* Y_{k_1}^{(N)}(\theta_1, \phi_1) \qquad (2.4.8)
 \end{aligned}$$

where $C_{k_0}(L, L')$ are the radiation parameters for radiation of multipole order L and L' . The arguments θ and ϕ of

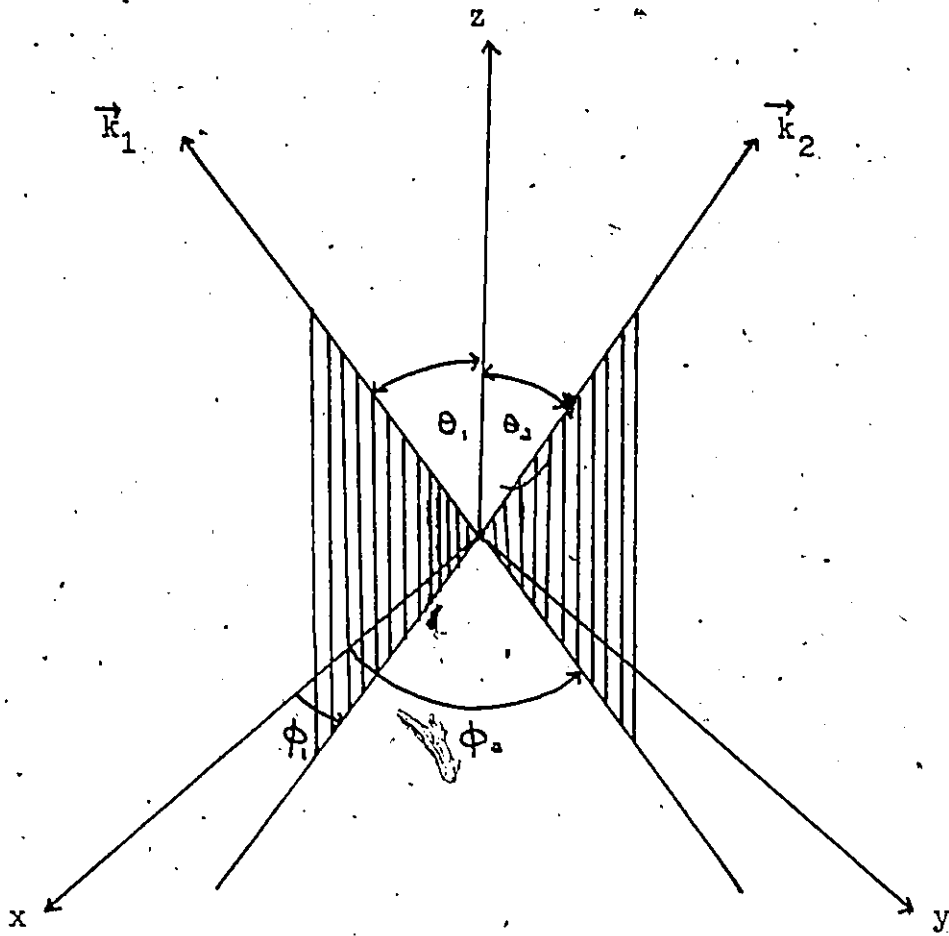


Fig. 2.4.1: Angular co-ordinates of the propagation directions \vec{k}_1 and \vec{k}_2 .

the spherical harmonics refer to the direction of observation of the radiation with respect to an arbitrarily chosen quantization axis z (Fig. 2.4.1).

A similar expression is obtained for

$$\sum_{m_f} \langle m_f | H_2 | m_b \rangle \langle m_f | H_2 | m_b' \rangle^*$$

The perturbed angular correlation function becomes:

$$W(\vec{k}_1, \vec{k}_2, t) = \sum_{\substack{k_1, k_2 \\ N_1, N_2}}^{K_{\max}} A_{k_1}(1) A_{k_2}(2) G_{k_1 k_2}^{N_1 N_2}(t) \\ \times \left[(2k_1 + 1)(2k_2 + 1) \right]^{-\frac{1}{2}} Y_{k_1}^{N_1}(\theta_1, \phi_1) Y_{k_2}^{N_2}(\theta_2, \phi_2) \quad (2.4.9)$$

where

$$G_{k_1 k_2}^{N_1 N_2}(t) = \sum_{m_a, m_b} (-1)^{2I + m_a + m_b} \left[(2k_1 + 1)(2k_2 + 1) \right]^{\frac{1}{2}} \\ \times \begin{pmatrix} I & I & k_1 \\ m_a' & -m_a & N_1 \end{pmatrix} \begin{pmatrix} I & I & k_2 \\ m_b' & -m_b & N_2 \end{pmatrix} \\ \times \langle m_b | \lambda(t) | m_a \rangle \langle m_b' | \lambda(t) | m_a' \rangle^* \quad (2.4.10)$$

The influence of the extranuclear perturbation is described by the perturbation factor $G_{k_1 k_2}^{N_1 N_2}(t)$.

$$A_{k_1}(1) = \sum_{L_1 L_1'} (-1)^{L_1} c_{k_0}^* (L_1 L_1') \begin{Bmatrix} I & I & k \\ L_1 & L_1' & I_1 \end{Bmatrix} \langle I \| L_1 \pi_1 \| I_1 \rangle \langle I \| L_1' \pi_1' \| I_1 \rangle^*$$

$A_{k_2}(2)$ is defined similarly.

The Eqn. (2.4.9) represents the time differential perturbed angular correlation i.e. the correlation measured if the second radiation is observed within time t and $t + dt$ after the emission of the first radiation.

In case of vanishing perturbation (indicated by $t = 0$) the evolution matrix reduces to the unit matrix and using Eqn. (A.6), the perturbation factor reduces to

$$G_{k_1 k_2}^{N_1 N_2} = \delta_{k_1 k_2} \delta_{N_1 N_2} \quad (2.4.11)$$

The unperturbed correlation function is thus obtained

$$W(\theta, 0) = \sum_k A_{kk} P_k(\cos \theta) \quad (2.4.12)$$

where $A_{kk} = A_k(1)A_k(2)$

and θ is the angle between k_1 and k_2 .

2.5 Static Interactions (Classical Fields):

For perturbed angular correlation caused by the interaction of nuclear magnetic or electric moments with a stationary external field which can be described classically, the matrix elements of $\lambda(t)$ can be expressed in the m-representation. Designating the unitary matrix which diagonalizes the interaction Hamiltonian K by U we get:

$$U K U^{-1} = E \quad (2.5.1)$$

E is the diagonal energy matrix with diagonal elements E_n (energy eigenvalues). By expansion of the exponential function, we obtain:

$$U e^{-iKt/\hbar} U^{-1} = e^{-iEt/\hbar} \quad (2.5.2)$$

Eqn.(2.4.6) then becomes

$$\lambda(t) = U^{-1} e^{-iEt/\hbar} U \quad (2.5.3)$$

and the matrix elements of $\lambda(t)$ in the m-representation are

$$\langle m_b | \lambda(t) | m_a \rangle = \sum_n \langle n | m_b \rangle^* \left[e^{-iE_n t/\hbar} \right] \langle n | m_a \rangle \quad (2.5.4)$$

where $\langle m | n \rangle$ are the matrix elements of the unitary matrix U that is obtained by solving Eqn. (2.5.1).

The perturbation factor is then:

$$\begin{aligned}
 G_{k_1 k_2}^{N_1 N_2}(t) = & \sum_{m_a, m_b} \sum_{n, n'} (-1)^{2I+m_a+m_b} \left[(2k_1+1)(2k_2+1) \right]^{\frac{1}{2}} \\
 & \times \exp[-i(E_n - E_{n'})t/\hbar] \langle n | m_b \rangle^* \langle n | m_a \rangle \\
 & \times \langle n' | m_b' \rangle \langle n' | m_a' \rangle^* \begin{pmatrix} I & I & k_1 \\ m_a' & -m_a & N_1 \end{pmatrix} \begin{pmatrix} I & I & k_2 \\ m_b' & -m_b & N_2 \end{pmatrix}
 \end{aligned}
 \tag{2.5.5}$$

z

If the field has axial symmetry eg. an axially symmetric electrostatic field, the symmetry axis of the interaction can be chosen parallel to z and used as the quantization axis for the eigenfunctions of the Hamiltonian K. The eigenfunctions are then simply $|m\rangle$ and K as well as $\lambda(t)$ are diagonal in this representation ($U=1$):

$$\langle m_b | \lambda(t) | m_a \rangle = \exp[-iE_m t/\hbar] \delta_{mm_a} \delta_{mm_b} \tag{2.5.6}$$

The perturbation factor Eqn. (2.4.10) then becomes:

$$\begin{aligned}
 G_{k_1 k_2}^{N_1 N_2}(t) = & \sum_m \left[(2k_1+1)(2k_2+1) \right]^{\frac{1}{2}} \begin{pmatrix} I & I & k_1 \\ m' & -m & N_1 \end{pmatrix} \begin{pmatrix} I & I & k_2 \\ m' & -m & N_2 \end{pmatrix} \\
 & \times \exp[-i(E_m - E_{m'})t/\hbar]
 \end{aligned}
 \tag{2.5.7}$$

Further, if the axially symmetric field is parallel to the propagation direction of the first radiation R_1 , then $Y_{k_1}^N(0, \phi)$ must be ϕ independent.

$$Y_{k_1}^N(0, \phi) = \delta_{N0} \left[(2k_1+1)(4\pi) \right]^{\frac{1}{2}}$$

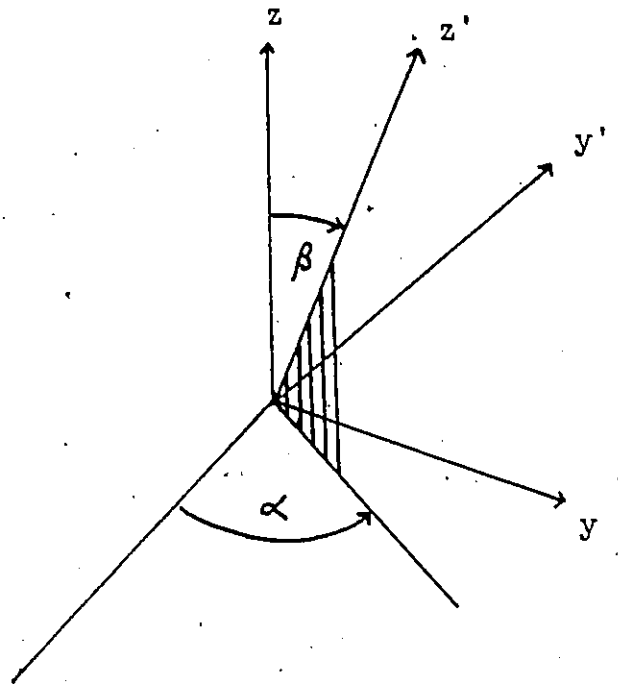


Fig.2.5.1: Position of z' axis defined by Euler angles α and β .

meaning

$$m = m' \quad \text{i.e.} \quad E_m - E_{m'} = 0$$

Using Eqn. (A.6) the Eqn. (2.5.7) reduces to

$$G_{k_1 k_2}^{N_1 N_2}(t) = \delta_{k_1 k_2} \quad (2.5.8)$$

Thus the angular correlation is not influenced by such a field as explained in Section 2.4.

In some cases angular correlation measurements are observed using radioactive sources that consist of an ensemble of randomly oriented microcrystals (powder source). If the angular correlation is perturbed by crystalline fields whose direction is related to the symmetry axis of the microcrystals, the observed angular correlation is obtained by averaging over random directions of the symmetry axes of the microcrystals. Assuming that the interacting fields in an individual are axially symmetric and denote this symmetric axis by z' . The interaction Hamiltonian is diagonal in the z' system:

$$K(z') = E_n \quad (2.5.9)$$

with eigenvalues E_n . The direction of the symmetry axis z' of the microcrystal is specified by the Euler angles $(\alpha, \beta, 0)$ with respect to the z -system (fig.2.5.1) The Hamiltonian in the z -system is obtained by applying

$$D^{(I)}(0, -\beta, -\alpha,) = D^{(I)-1}(\alpha, \beta, 0)$$

$$K(z) = D^{(I)-1}(\alpha, \beta, 0) K(z') D^{(I)}(\alpha, \beta, 0) \quad (2.5.10a)$$

Since $K(z')$ is diagonal, we can also write

$$D^{(I)}(\alpha, \beta, 0) K(z) D^{(I)-1}(\alpha, \beta, 0) = K(z') = E_n \quad (2.5.10b)$$

corresponding to Eqn. (2.5.1)

Therefore, the unitary transformation $D^{(I)}(\alpha, \beta, 0)$

diagonalizes $K(z)$. The matrix elements of the evolution operator $\lambda(t)$ in the m -representation are thus according to Eqn. (2.5.4):

$$\langle m_b | \lambda(t) | m_a \rangle = \sum_n D_{n, m_b}^{(I)*} \left[\exp -iE_n t/\hbar \right] D_{n m_a}^{(I)} \quad (2.5.11)$$

and the perturbing factor is

$$G_{k_1 k_2}^{N_1 N_2}(t) = \sum_{m_a, m_b} \sum_{n, n'} \left[(2k_1+1)(2k_2+1) \right]^{\frac{1}{2}} (-1)^{2I+m_a+m_b} \\ \times \begin{pmatrix} I & I & k_1 \\ m'_a & -m_a & N_1 \end{pmatrix} \begin{pmatrix} I & I & k_2 \\ m'_b & -m_b & N_2 \end{pmatrix} \\ \times D_{n m_b}^{(I)*} D_{n m_a}^{(I)} D_{n' m'_b}^{(I)*} D_{n' m'_a}^{(I)*} \exp -i(E_n - E_{n'})t/\hbar \quad (2.5.12)$$

Using the general contraction relation, the summation over m_a and m_b can be performed

$$\sum_{m_a} \begin{pmatrix} I & I & k_1 \\ m'_a & -m_a & N_1 \end{pmatrix} D_{n', m'_a}^{(I)*} D_{-n, -m_a}^{(I)*} = \begin{pmatrix} I & I & k_1 \\ n' & -n & p_1 \end{pmatrix} D_{p_1, N_1}^{(k_1)} \quad (2.5.13)$$

And similarly for $\sum m_b$

Integrating over the Euler angles α and β yields

$$\begin{aligned} \overline{G_{k_1 k_2}^{N_1 N_2}}^{\alpha, \beta}(t) &= 1/4 \left[(2k_1+1)(2k_2+1) \right]^{\frac{1}{2}} \sum_{n, n'} \begin{pmatrix} I & I & k_1 \\ n' & -n & p_1 \end{pmatrix} \begin{pmatrix} I & I & k_2 \\ n' & -n & p_2 \end{pmatrix} \\ &\times \exp -i(E_n - E_{n'})t/\hbar \\ &\times \int_0^{2\pi} \int_0^\pi D_{p_1 N_1}^{k_1}(\alpha, \beta, 0) \times D_{p_2 N_2}^{k_2*}(\alpha, \beta, 0) d\alpha \sin\beta d\beta \end{aligned} \quad (2.5.14)$$

By virtue of the orthogonality of the D-functions the integral reduces to

$$4\pi (2k_1+1)^{-1} \delta_{k_1 k_2} \delta_{p_1 p_2} \delta_{N_1 N_2}$$

The perturbation factor of the powder source is

$$\overline{G_{kk}}^{\alpha, \beta}(t) = \overline{G_{k_1 k_2}^{N_1 N_2}}^{\alpha, \beta}(t) = \frac{1}{(2k+1)} \sum_N G_{k, k}^{N, N}(t) \quad (2.5.15)$$

This equation has been derived from

$$G_{kk}(t) = \overline{G_{k_1 k_2}^{N_1 N_2}(t)}^{\alpha, \beta} = \sum_{n, n'} \left(\begin{matrix} I & I & k \\ n' & -n & p \end{matrix} \right)^2 e^{-i(E_n - E_{n'})t/\hbar} \quad (2.5.16)$$

by comparison with Eqn. (2.5.7).

If the interacting fields in the individual microcrystals are not axially symmetric with respect to some crystalline axis z' , then the interaction Hamiltonian $K(z')$ is not diagonal. Denoting the unitary transformation that diagonalizes $K(z')$ by U , then Eqn. (2.5.10) must be changed to

$$U D^{(I)}(\alpha, \beta, \gamma) K(z) D^{(I)-1}(\alpha, \beta, \gamma) U^{-1} = U K(z') U^{-1} = E \quad (2.5.17)$$

In the derivation of the perturbation factor for powder sources, the matrix element $\langle n | m \rangle$ of U must be carried along in the calculation of $G_{kk}(t)$. The resulting perturbation factor for a non-axially symmetric interaction in the micro-crystals becomes

$$G_{k,k}(t) = \overline{G_{k_1 k_2}^{N_1 N_2}(t)}^{\alpha, \beta, \gamma} = \sum_{N_1, m_a, m_b} \sum_{n_1, n'} (-1)^{2I+m_a+m_b} \times \begin{pmatrix} I & I & k \\ m'_a & -m_a & N \end{pmatrix} \begin{pmatrix} I & I & k \\ m'_b & -m_b & N \end{pmatrix} \times \exp-i(E_n - E_{n'})t/\hbar$$

$$x \langle n | m_b \rangle^* \langle n | m_a \rangle \langle n' | m_b' \rangle \langle n' | m_a' \rangle^* \quad (2.5.18)$$

which can again be put in the form

$$G_{k,k}(t) = \overline{G_{k_1, k_2}^{N_1, N_2}(t)}_{\alpha, \beta, \gamma} = \frac{1}{(2k+1)} \sum_{N=-k}^k G_{k,k}^{N,N}(t) \quad (2.5.18b)$$

Since $G_{kk}(t)$ is independent of N_1, N_2 , the addition theorem of spherical harmonics can be applied to Eqn.(2.4.9) and the directional correlation displayed by a powder source has the form

$$W_p(\theta, t) = \sum_k A_k(1) A_k(2) G_{kk}(t) P_k(\cos \theta) \quad (2.5.19)$$

the effect of the randomly oriented perturbation does not change the form of the angular correlation. It only attenuates the coefficient of the $P_k(\cos \theta)$. The perturbation factors $G_{kk}(t)$ for sources that as a whole display no privileged direction are called attenuation factors.

2.6 Static Electric Quadrupole Interaction:

My work for this thesis is based on the perturbation due to this interaction.

The Hamiltonian describing the interaction of a fixed electrostatic gradient with the electric quadrupole moment of the nucleus is given by:

$$K_Q = 4/5 \pi T^{(2)} V^{(2)} = 4/5 \pi \sum_q (-1)^q T_q^{(2)} V_{-q}^{(2)} \quad (2.6.1)$$

where $T^{(2)}$ is the second rank tensor operator of the nuclear quadrupole moment with the components:

$$T_q^{(2)} = \sum_p e_p r_p^2 Y_2^q(\theta_p, \phi_p) \quad (2.6.2)$$

where e_p are the point charges in the nucleus at points (r_p, θ_p, ϕ_p) . $V^{(2)}$ is the tensor operator of the classically external field gradient.

If the electrostatic field is caused by point charges e_c (ions in a crystal lattice) at positions (r_c, θ_c, ϕ_c) with respect to the nuclear centre, the spherical components of the field tensor $V^{(2)}$ are given by:

$$V_q^{(2)} = \sum_c e_c / r_c Y_2^q(\theta_c, \phi_c) \quad (2.6.3)$$

or in terms of arbitrary cartesian co-ordinate system

x', y', z' the components are

$$\begin{aligned} V_0^{(2)} &= \frac{1}{4} \sqrt{\frac{5}{\pi}} V_{z'z'} \\ V_{\pm 1}^{(2)} &= \mp \frac{1}{2} \sqrt{\frac{5}{6\pi}} (V_{x'z'} \pm iV_{y'z'}) \\ V_{\pm 2}^{(2)} &= \frac{1}{4} \sqrt{\frac{5}{6\pi}} (V_{x'x'} - V_{y'y'} \pm 2iV_{x'y'}) \end{aligned} \quad (2.6.4)$$

If the co-ordinate system (x, y, z) is chosen such that the mixed derivatives of the potential V disappears:

$$\begin{aligned} V_0^{(2)} &= \frac{1}{4} \sqrt{\frac{5}{\pi}} V_{zz} \\ V_{\pm 1}^{(2)} &= 0 \end{aligned} \quad (2.6.5)$$

$$V_{\pm 2}^{(2)} = \frac{1}{4} \sqrt{\frac{5}{6\pi}} (V_{xx} - V_{yy}) = \frac{1}{4} \sqrt{\frac{5}{6\pi}} \eta V_{zz}$$

where the asymmetry parameter η of the electric field is defined as

$$\eta = \frac{V_{xx} - V_{yy}}{V_{zz}} \quad (2.6.6)$$

Choose the principal axes system such that

$$|V_{xx}| < |V_{yy}| < |V_{zz}|$$

restricts η to $0 < \eta < 1$, because of Poisson's equation:

$$V_{xx} + V_{yy} + V_{zz} = 0.$$

The gradient tensor $v^{(2)}$ is then determined by the parameter η and V_{zz} .

When the fields are axially symmetric with respect to the z-axis $\eta = 0$.

$$v_{\pm 2}^{(2)} = v_{\pm 1}^{(2)} = 0;$$

$$v_0^{(2)} = \left(\frac{5}{16}\pi\right)^{\frac{1}{2}} V_{zz}$$

The interaction Hamiltonian is then

$$K_Q = \sqrt{\frac{\pi}{5}} T_0^{(2)} V_{zz} \quad (2.6.7)$$

The matrix elements of this Hamiltonian in the m-representation are obtained by applying the Wigner-Eckart theorem:

$$\begin{aligned} \langle I_m | K_Q | I_{m'} \rangle &= \sqrt{\frac{\pi}{5}} V_{zz} \langle I_m | T_0^{(2)} | I_{m'} \rangle \\ &= \sqrt{\frac{\pi}{5}} V_{zz} (-1)^{I-m} \begin{pmatrix} I & 2 & I \\ -m & 0 & m' \end{pmatrix} \langle I || T^{(2)} || I \rangle \end{aligned} \quad (2.6.8)$$

The 3 - j symbol vanishes for $m \neq m'$, the matrix K_Q is diagonal.

The conventional definition of the electric quadrupole

Q is:

$$eQ = \left\langle II \left| \sum_p e_p (3z_p^2 - r_p^2) \right| II \right\rangle \quad (2.6.9)$$

or

$$eQ = 4\sqrt{\frac{II}{5}} \left\langle II \left| T_0^{(2)} \right| II \right\rangle \quad (2.6.10)$$

Applying Wigner-Eckart theorem we get:

$$eQ = 4\sqrt{\frac{II}{5}} \begin{pmatrix} I & 2 & I \\ -I & 0 & I \end{pmatrix} \left\langle I \left\| T_0^{(2)} \right\| I \right\rangle \quad (2.6.11)$$

After the evaluation of the 3-j symbols, the quadrupole interaction matrix elements are:

$$\left\langle I_m \left| K_Q \right| I_m \right\rangle = E_m = \frac{(3m^2 - I(I+1)) eQV_{zz}}{4I(2I-1)} \quad (2.6.12)$$

Introducing the quadrupole frequency, we obtain:

$$w_Q = \frac{-eQV_{zz}}{4I(2I-1)\hbar} \quad (2.6.13)$$

$$E_m = \left[I(I+1) - 3m^2 \right] w_Q \hbar \quad (2.6.14)$$

Let the angular frequency corresponding to the smallest non-vanishing energy difference be w_0 , then

$$w_0 = 3w_Q \quad \text{for integral I}$$

$$w_0 = 6w_Q \quad \text{for half-integral I}$$

The energy splittings due to the static quadrupole interaction are not uniform as mentioned in Section 2.4.

Thus the influence of a quadrupole interaction on an angular correlation cannot be described semi-classically by a simple precession of the correlation pattern.

The perturbation factor for the static electric quadrupole interaction is according to Eqn. (2.5.7):

$$G_{k_1 k_2}^{N_1 N_2}(t) = \sum_m [(2k_1+1)(2k_2+1)]^{\frac{1}{2}} \begin{pmatrix} I & I & k_1 \\ m' & -m & N \end{pmatrix} \begin{pmatrix} I & I & k_2 \\ m' & -m & N \end{pmatrix} \times \exp(-3i(m^2 - m'^2)w_Q t) \quad (2.6.15)$$

Since the exponential term depends on the summation index m , the orthogonality of the 3-j symbols cannot be used to eliminate the interference term with $k_1 \neq k_2$. Thus the interference factors $A_{k_1}(1)A_{k_2}(2)$ must be computed from the factors $A_{k_1}(1)$ and $A_{k_2}(2)$, which must be known individually. This needs an accurate knowledge of the multipole expansion of the two radiations involved in the cascade.

From Eqn. (2.6.15) if k_1 or k_2 is zero, then

$N = 0$ and this implies that $m' = m$.

When $m' = m$, the exponential term is unity and using the orthogonality of the 3-j symbols results in the vanishing of the perturbation factor. Thus, the interference term occurs only if $k_{\max} \geq 4$.

The perturbation factor of Eqn. (2.6.15) can be written as

$$G_{k_1 k_2}^{N_1 N_2}(t) = \sum_n S_{n N}^{k_1 k_2} \cos(n\omega_0 t) \quad (2.6.16)$$

with

$$S_{n N}^{k_1 k_2} = \sum_{\substack{m \\ m'}}' \begin{pmatrix} I & I & k_1 \\ m' & -m & N \end{pmatrix} \begin{pmatrix} I & I & k_2 \\ m' & -m & N \end{pmatrix} \times \left[(2k_1+1)(2k_2+1) \right]^{\frac{1}{2}} \quad (2.6.17)$$

where the prime on the summation sign shows that the summation over m and m' should include those terms where m and m' satisfy the conditions:

$$\begin{aligned} |m^2 - m'^2| &= n && \text{for integer } I \\ \frac{1}{2}|m^2 - m'^2| &= n && \text{for half-integer } I \end{aligned} \quad (2.6.18)$$

Values of the coefficients $S_{n N}^{k_1 k_2}$ have been calculated for some cases. With these the directional correlation perturbed by an axially symmetric electrostatic gradient in an arbitrary direction (eg. for a non-cubic crystal

source) can be found.

For a polycrystalline powder source, the effect of an axially symmetric quadrupole interaction on the angular correlation measurements is represented by the attenuation coefficients given in Eqn. (2.5.15)

$$G_{kk}(t) = \sum_{m', m} \left(\begin{matrix} I & I & k \\ m' & -m & p \end{matrix} \right)^2 \exp \left[-3i (m^2 - m'^2) w_Q t \right]$$

The calculation of these coefficients for powder sources where the perturbation is the result of rhombic fields is more complicated. The rhombic field Hamiltonian must be diagonalized and the eigenvalues and eigenfunctions must be determined for various values of w_Q and η . The attenuation coefficients can then be calculated from Eqn. (2.5.18).

It has been assumed so far that the electric field gradients acting on the nuclear quadrupole moments are identical at every nuclear site. But, in reality slight variations of the crystalline fields occur due to lattice imperfections and impurity centers. The radioactive decay process transforms the atom in a lattice to an impurity center in most cases. Also, the recoil momentum displaces the atom from its regular lattice position to a less well-defined position. This results in variations of the crystalline fields experienced by the nuclei in the intermediate state.

This variation results in a probability distribution $P(w_0)$ of the quadrupole interaction frequency w_0 . The frequency distribution is assumed to be a normal distribution.

$$P(w_0)dw_0 = \frac{1}{\sqrt{2\pi}\sigma} \exp \left[- \left\{ (w_0 - w_0^0) / \sqrt{2}\sigma \right\}^2 \right] dw_0 \quad (2.6.19)$$

w_0^0 is the centroid

σ is the width of the distribution.

The frequency averaged perturbation factor is then

$$q_{k_1 k_2}^{N_1 N_2}(w_0^0 t) = \frac{\int G_{k_1 k_2}^{N_1 N_2}(w_0 t) P(w_0) dw_0}{\int P(w_0) dw_0} \quad (2.6.20)$$

The relative width σ/w_0^0 is defined as the smearing delta δ .

2.7 Adaptation of Theoretical Results for Experiment:

(a) Theoretical Results:

As seen in Section 2.4 the directional correlation function $W(\theta)$ can be expressed as:

$$W(\theta) = \sum_{k \text{ even}} A'_{k k} P_k(\cos \theta) \quad (2.7.1)$$

where

$$A'_{k k} = A'_{k (L_1 L'_1 I_i I)} A'_{k (L_2 L'_2 I_f I)} \quad (2.7.2)$$

and

$$A'_{k (L_1 L'_1 I_i I)} = \sum_{L_1 L'_1} (-1)^{L_1} C_{k0}^{*L_1}(L_1 L'_1) \left\{ \begin{matrix} I & I & k \\ L_1 & L'_1 & I_i \end{matrix} \right\} \\ \times \langle I \parallel L_1 \Pi_1 \parallel I_i \rangle \langle I \parallel L'_1 \Pi'_1 \parallel I_i \rangle^* \quad (2.7.3)$$

$$A'_{k (L_2 L'_2 I_f I)} = \sum_{L_2 L'_2} (-1)^{L_2} C_{k0}^{*L_2}(L_2 L'_2) \left\{ \begin{matrix} I & I & k \\ L_2 & L'_2 & I_f \end{matrix} \right\} \\ \times \langle I \parallel L_2 \Pi_2 \parallel I_f \rangle^* \langle I \parallel L'_2 \Pi'_2 \parallel I_f \rangle \quad (2.7.4)$$

The coefficients $A'_{k k}$ in Eqn. (2.7.1) are not normalized. Normalization can be done using the equations (2.7.2), (2.7.3) and (2.7.4) by dividing each coefficient $A'_{k k}$ by A'_{00} .

Thus we get:

$$W(\theta) = 1 + A_{22} P_2(\cos \theta) + A_{44} P_4(\cos \theta) + \dots + A_{k_{\max} k_{\max} k_{\max}} P_{k_{\max}}(\cos \theta) \quad (2.7.5)$$

where $A_{kk} = A'_{kk} / A'_{00}$

Eqn. (2.7.5) holds for both pure and mixed multipoles and the first treatment of multipoles was done in 1949 (Ling & Falkoff, 1949).

Consider a γ - γ cascade in which two multipole components L_n and L'_n contribute to each of the two gamma transitions as in this work. Equation (2.7.5) maintains the same form, except that the coefficients A_{kk} undergo modification and become:

$$A_k(L_1 L'_1 I_i I) = \left[F_k(L_1 L_1 I_i I) + 2\Delta_1(\gamma) F_k(L_1 L'_1 I_i I) + \Delta_1^2(\gamma) F_k(L'_1 L'_1 I_i I) \right] / [1 + \Delta_1^2(\gamma)] \quad (2.7.6)$$

with a similar expression for $A_k(L_2 L'_2 I_f I)$

where

$$F_k(L_1 L'_1 I_i I) = A'_k(L_1 L_1 I_i I) / A'_0(L_1 L'_1 I_i I) \quad (2.7.7)$$

and $\Delta_1(\gamma)$ is the amplitude mixing ratio of the first transition defined as the ratio of the reduced matrix elements

$$\Delta_1(\gamma) \equiv \langle I \| L'_1 \Pi'_1 \| I_i \rangle / \langle I \| L_1 \Pi_1 \| I_i \rangle \quad (2.7.8)$$

$\Delta_2(\gamma)$ is similarly defined.

2.7 (b) Experimental Formulae:

The directional correlation function $W(\theta, t)$ used in this thesis given in Eqn. (2.4,9) has been modified by Dr. Ogata to take into consideration the lattice imperfections of the crystal. The Eqn. (2.4.9) is true only for a perfect crystal. The modified form is:

$$\begin{aligned}
 W(\theta, t) = & \sum_{k_1=0,2,4} \sum_{N_1=-k_1}^{k_1} \sum_{m_a, m'_a=-I}^I (-1)^{I+m_a} \\
 & \times A_{k_1} P_{k_1}^{N_1}(\cos \theta_1) \begin{pmatrix} I & I & k_1 \\ m_a & -m'_a & N_1 \end{pmatrix} \\
 & \times \sum_{k_2=0,2,4} \sum_{N_2=-k_2}^{k_2} \sum_{m_b, m'_b=-I}^I (-1)^{I+m_b} \\
 & \times A_{k_2} P_{k_2}^{N_2}(\cos \theta_2) \begin{pmatrix} I & I & k_2 \\ m_b & -m'_b & N_2 \end{pmatrix} \exp(-iN_2\phi) \\
 & \times \sum_{n=-I}^I \sum_{n'=-I}^I \langle n | m_a \rangle \langle n' | m'_a \rangle^* \langle n | m_b \rangle \langle n' | m'_b \rangle^* \\
 & \times \left\langle \left\langle \exp(-i(E(n) - E(n'))t) \right\rangle_{Av}^w \right\rangle_r^t \quad (2.7.9)
 \end{aligned}$$

where t_r is the response time of the time-to-amplitude converter. A_{ki} ($k = 0, 2, 4, i = 1, 2$) are the correlation coefficients defined in Eqns. (2.7.3) - (2.7.4).

The measured correlation function is taken for two values of θ , i.e. 180° and 90° . The final result is expressed as the experimental anisotropy $R^{\text{exp}}(t)$ defined as:

$$R^{\text{exp}}(t) = 2 \left[W(\pi) - W(\pi/2) \right] / \left[W(\pi) + W(\pi/2) \right] \quad (2.7.10)$$

The experimental results yield w_0 and this value together with the knowledge of the nuclear quadrupole moment Q will give rise to an average value of V_{zz} from Eqn. (2.6.13).

CHAPTER III

EXPERIMENT

3.1 Introduction:

In angular correlation work, a typical situation is as follows: a nucleus emits in rapid succession two gamma-rays γ_1 and γ_2 . We ask for the relative probability $W(\theta)d\Omega$ that γ_2 is emitted into the solid angle $d\Omega$ at an angle θ with respect to \vec{k}_1 . The theoretical expression for the correlation function $W(\theta')$ for γ -rays has already been discussed in Chapter II. Experimentally, the number of coincidences between γ_1 and γ_2 are recorded as a function of the angle θ' between the axes of the two counters. Because of the finite solid angles of the counters, these numbers $C(\theta')$ are average of the true correlation $W(\theta)$ over angles θ distributed around θ' . (Fig. 3.1.1). Hence the $C(\theta')$ must be properly corrected and normalized to yield $W_{\text{exp}}(\theta)$. The comparison of $W_{\text{exp}}(\theta)$ with theory finally provides the desired information.

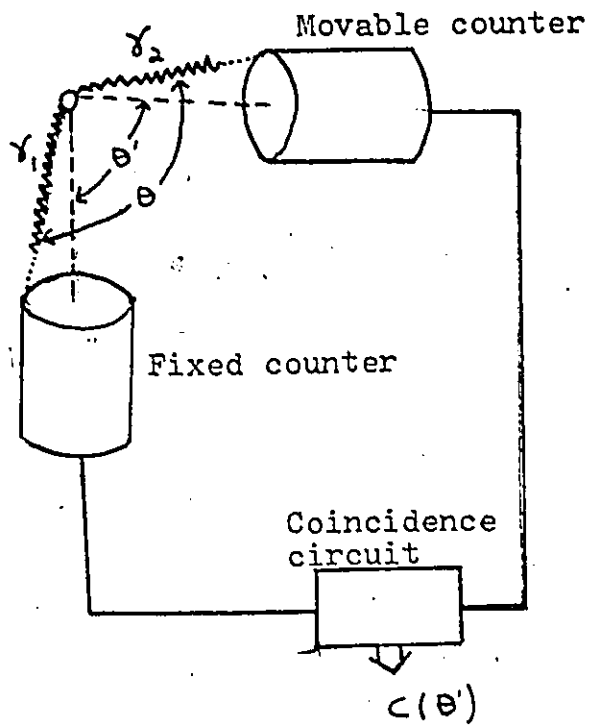


Fig. 3.1.1. Simple Coincidence Circuit

3.2 Experimental Correlation Function:

This section deals with the relation of the theoretical perturbed correlation function discussed in Chapter II with the experimental correlation $R(\theta)$. Let N and C denote the single counts and coincidences respectively. From measured data, the "true" values $C^t(\theta)$ and $N^t(\theta)$ are obtained by subtracting the background and accidental coincidences. This can be expressed as :

$$C^t(\theta) = C^{\text{meas}}(\theta) - C^{\text{acc}}(\theta) \quad (3.2.1)$$

where

$$C^{\text{acc}}(\theta) = 2 \tau_0 N_1^{\text{meas}}(\theta) N_2^{\text{meas}}(\theta) \quad (3.2.2)$$

where θ denotes the angles between γ_1 and γ_2 .

τ_0 is the resolving time per channel

The reason for the accidental coincidences is that, because of the large number of nuclei decaying in the source, it is possible that a γ_1 from one nucleus will occur in coincidence with a γ_2 from another nucleus. The true number of single counts and coincidences can be written as:

$$N_i^t = N_0 p_i \Omega_i \epsilon_i \quad (3.2.3)$$

$$C^t(\theta) = N_0 p_1 p_2 \Omega_1 \epsilon_1 \Omega_2 \epsilon_2 \epsilon_c R(\theta) \quad (3.2.4)$$

where

N_0 : number of disintegrations per unit time

p_i : probability per disintegration that the radiation selected in counter is emitted

Ω_i : the solid angle in units of 4π

ϵ_i : the efficiency of the counter i

ϵ_c : the efficiency of the coincidence circuit

$R(\theta)$: the experimental correlation function

Due to the finite deadtime of the time-to-amplitude-converter (TAC) some pulses are not analysed, so that ϵ_c is not unity. But since the activity of the source was not very high ϵ_c may be taken as unity. The ratio of the coincidences to the single is given by:

$$\begin{aligned} \text{Ratio} &= \frac{\text{Coincidences}}{N_{y_1}^t(\theta) N_{y_2}^t(\theta)} \\ &= \frac{N_0 p_1 p_2 \Omega_1 \epsilon_1 \Omega_2 \epsilon_2 \epsilon_c R(\theta)}{(N_0 p_1 \Omega_1 \epsilon_1)(N_0 p_2 \Omega_2 \epsilon_2)} \\ &= \frac{R(\theta)}{N_0} \quad \text{if } \epsilon_c = 1 \end{aligned}$$

Therefore, $R(\theta) = N_0 \times \text{ratio}$

$$= N_0 \frac{c^t(\theta)}{N_1^t(\theta) N_2^t(\theta)} \quad (3.2.5)$$

The experimental anisotropy is given by:

$$R^{\text{exp}}(t) = 2 \left[\frac{f(\pi) - f(\pi/2)}{f(\pi) + f(\pi/2)} \right]$$

thus becomes upon substitution of Eqn. (3.2.5)

$$R^{\text{exp}}(t) = 2 \left[\frac{\frac{N_o(t_o)C^t(\pi)}{N_{\gamma_1}^t(\pi)N_{\gamma_2}^t(\pi)} - \frac{N'_o(t_1)C^t(\pi/2)}{N_{\gamma_1}^t(\pi/2)N_{\gamma_2}^t(\pi/2)}}{\frac{N_o(t_o)C^t(\pi)}{N_{\gamma_1}^t(\pi)N_{\gamma_2}^t(\pi)} + \frac{N'_o(t_1)C^t(\pi/2)}{N_{\gamma_1}^t(\pi/2)N_{\gamma_2}^t(\pi/2)}} \right] \quad (3.2.6)$$

where

$N_o(t_o)$: the disintegration rate at time t_o

$N'_o(t_1)$: the disintegration rate at time t_1

$t_1 - t_o$: the mean time between the accumulation of data at 180° and 90° .

Corrections are made for the time difference between the collection of data at 180° and 90° .

If the disintegration constant is λ

then we have:

$$N'_o(t_1) = N_o(t_o) \exp[-\lambda(t_1 - t_o)]$$

Therefore

$$R^{\text{exp}}(t) = 2 \left[\frac{C^t(\pi)}{N_{\gamma_1}^t(\pi)N_{\gamma_2}^t(\pi)} - \frac{C^t(\pi/2)}{N_{\gamma_1}^t(\pi/2)N_{\gamma_2}^t(\pi/2)\exp\lambda(t_1-t_0)} \right. \\ \left. \frac{C^t(\pi)}{N_{\gamma_1}^t(\pi)N_{\gamma_2}^t(\pi)} + \frac{C^t(\pi/2)}{N_{\gamma_1}^t(\pi/2)N_{\gamma_2}^t(\pi/2)\exp\lambda(t_1-t_0)} \right]$$

(3.2.7)

This equation was used in the calculation of anisotropy.

3.3 Apparatus:

The directional correlation of the (132 keV and 480 keV) γ - γ cascade in ^{181}Ta was observed time differentially using a two detector fast-slow coincidence technique. The scintillation detectors used were 2"x2" and $\frac{1}{4}$ "x2" thallium activated sodium iodide crystals mounted on 56AVP photomultipliers. The large crystal detected the 480 keV γ -ray while the smaller crystal detected the 132 keV γ -ray. This selection of crystals reduced the random coincidence rate.

The fixed counter 1 was placed at a distance of 8.2 cm. from the source while the movable counter 2 at a distance of 6.3 cm. for the 180° -detector position and at a distance of 6.2 cm. for the 90° -detector position. Lateral lead shielding was used to minimize coincidence due to scattering. The experimental set-up is shown in Fig. (3.3.1)

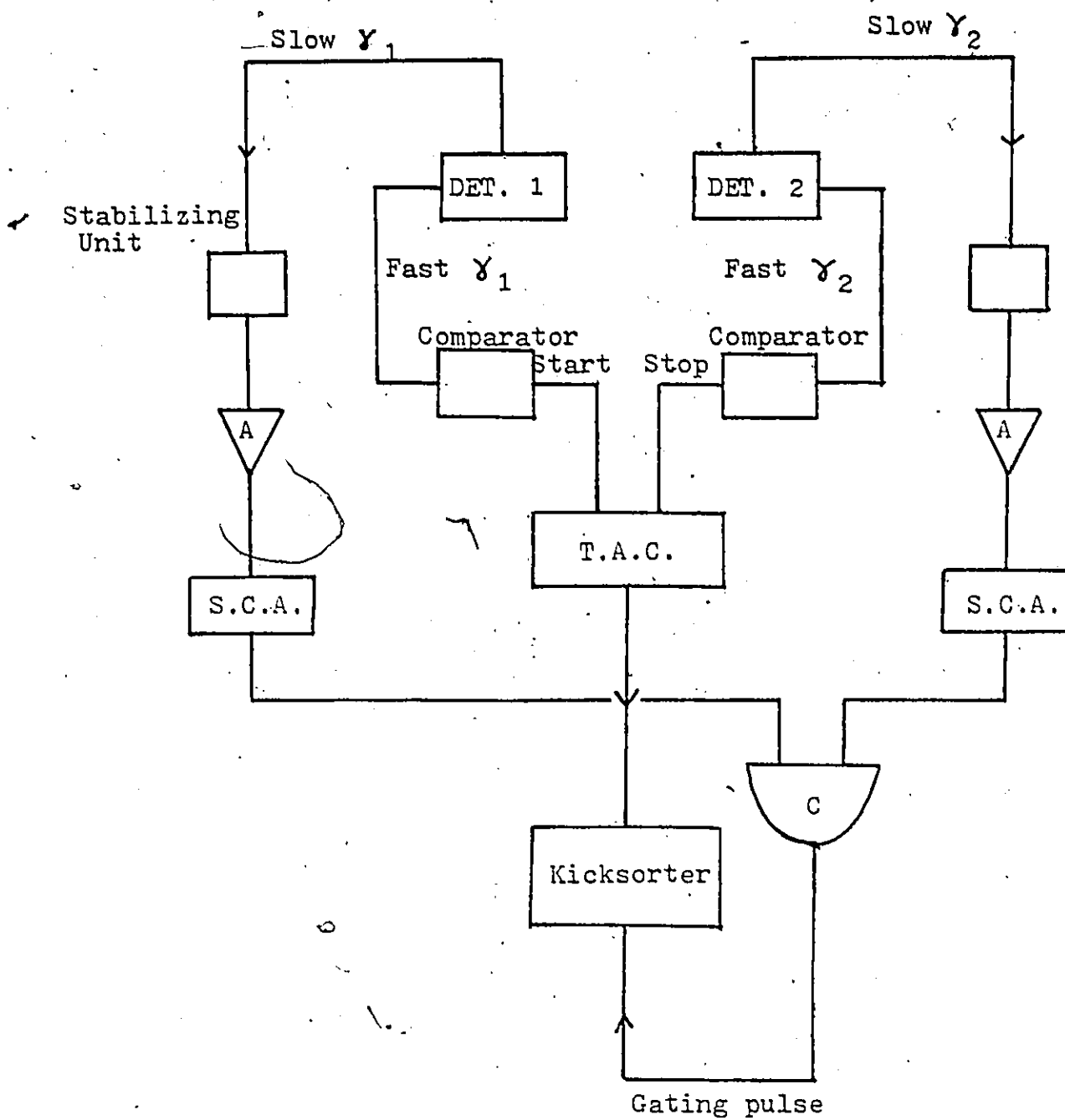


Fig. 3.3.1 Block Diagram of Apparatus.

3.4 Working of the Apparatus:

First, consider the fast pulse system. The pulse output from the anode of the photomultiplier tube was fed into the comparator to minimize noise due to thermal emission of electrons. This was done by setting the comparator at some specific voltage to which all input pulses were compared. A pulse was formed in the comparator when the amplitude of the input pulse was greater than the set voltage. This procedure was carried out for both detectors. The output pulse from comparator 1 was used as the start pulse for the time-to-amplitude convertor, Ortec Model 447. The pulse from comparator 2 was delayed by 30 ns by means of a length of cable (Amphenol Canada-RG 58 A/V Serial 03554) and used as the stop pulse. Thus the TAC was used to determine the time interval between the γ_1 and γ_2 pulses. The output of the TAC was fed to the multichannel analyser.

5 Now consider the slow pulse system. The slow pulse output taken from the tenth dynode was fed to a stabilizing unit to minimize drift. The resulting pulses were then amplified and fed to the single channel analysers. These single channel analysers were used to select the 132 keV and 480 keV pulses forming the cascade. (See Fig. 3.4.1). The procedure for this selection is as follows: the slow pulses

were fed through a 2 μ s delay line (Technical Measurement Corporation, Model 404) to the kicksorter, which was gated by the output of the single channel analyser. In this way only those pulses accepted by the window of the single channel analyser were analysed. Thus the windows were set to analyse the photopeaks of the 132 keV and 482 keV gamma rays.

The next step after the adjustment of the single channel analysers was time analysis. The outputs of the single channel analysers were fed into the double coincidence circuit. The resulting output was used to gate the kicksorter. As mentioned previously, the output of the TAC was also sent to the multi-channel analyser. Thus the spectrum produced was the coincidence rate as a function of time, the channel number being proportional to time.

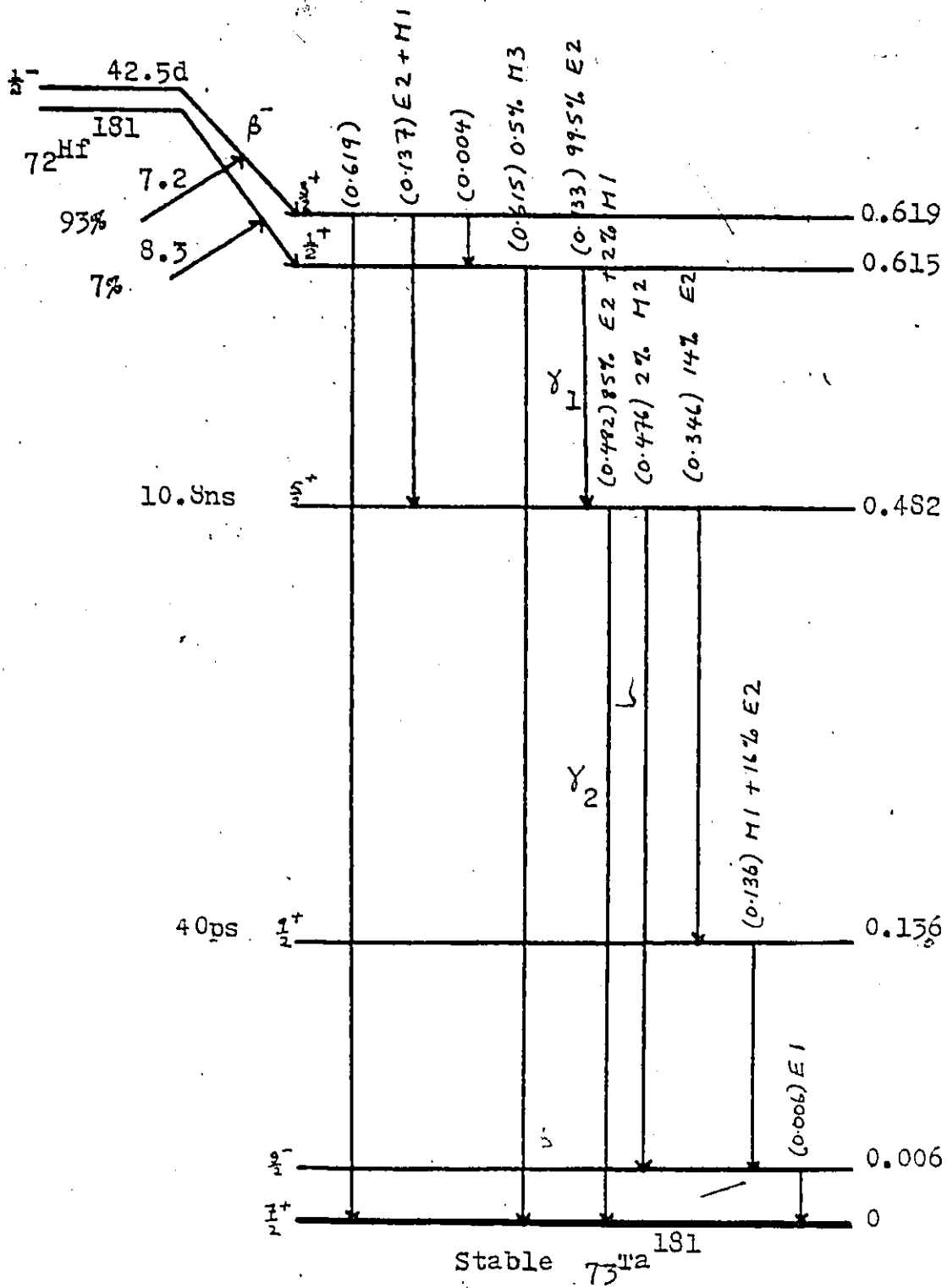


Fig. 5.4.1 Hf^{181} Decay Scheme (Table of Isotones)
(Not drawn to scale)

Time Calibration:

The time calibration was carried out by the method described by Bell (Bell, 1952). Using the same apparatus the number of channels corresponding to each rotation of the delay line was determined. Using the method of centroids it was found that one channel was equivalent to about 0.936 ns. Typical calibration results are shown in Table I

Time Zero Calibration:

By introducing the delay cable in the experimental arrangement the time-zero point was shifted. Therefore, it was necessary to evaluate the channel corresponding to the time zero point. To do this the coincidence experiment using the ^{60}Co decay was carried out. This was carried out using the same windows that were set in the time to amplitude convertor experiment.

The source was chosen because its mean life-time in the intermediate state is only 0.7 ps. (Fig. 3.4.2). Thus coincidence counting for only time-zero on the coincidence time spectrum is expected. However, this is only true for an ideal case. Due to fluctuations of a statistical nature in the emission of photons in the scintillation counter and other instrumental effects, there was a definite spread of coincidence counting

about time zero. Thus, this experiment with the ^{60}Co source determined not only time zero but also found the resolving time of the coincidence apparatus. The resolving time was taken as the full width at half maximum. (Fig. 3.4.3). The resolving time was found experimentally to be 4.48 ns.

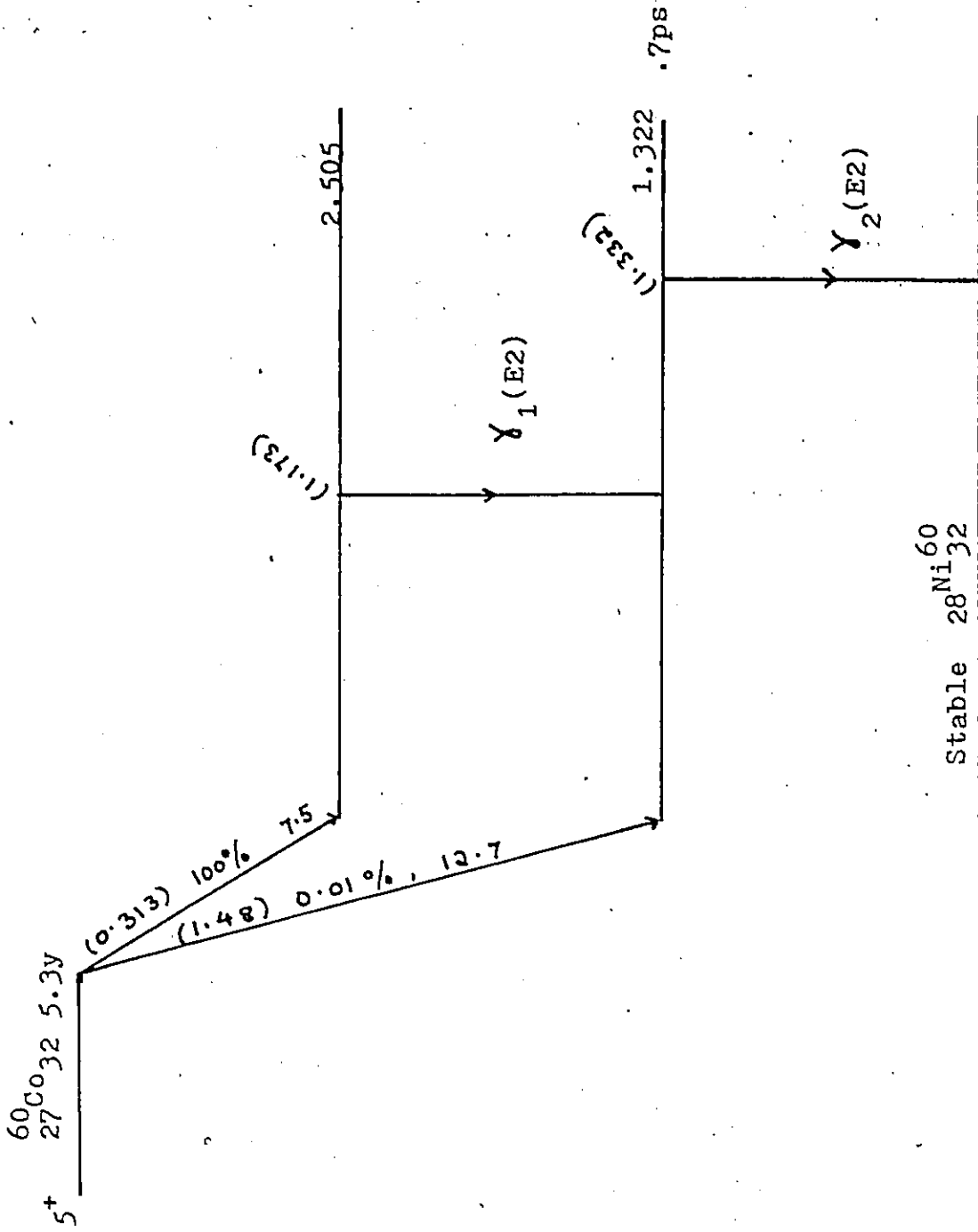


Fig.3.4.2: Decay scheme of ^{60}Co

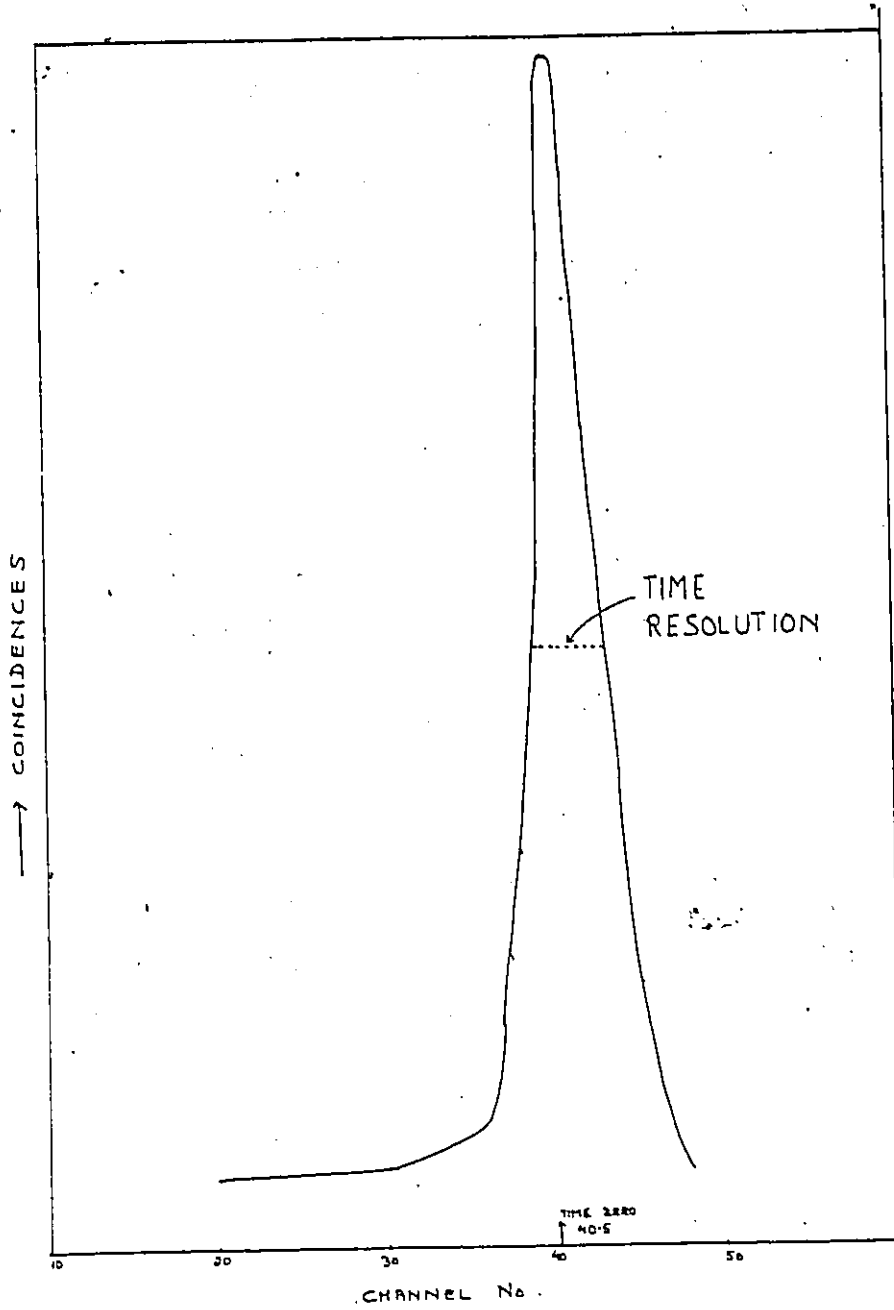


Fig.(3.4.3): ^{60}Co Run

3.5 Experimental Procedure:

The crystal was mounted so that the crystal was parallel to detector 1 and in the plane of detectors 1 and 2. This was done by mounting the crystal with the sides containing the frames facing the fixed detector. (refer to Figs. 3.5.1 & 3.5.2). It was then rotated through 45° . The windows were adjusted as described in Section 3.4. Finally the apparatus was set up for the time analysis i.e. the accumulation of the coincidence -time spectrum. Depending upon the activity of the source (half-life of Hf-181 is 45d) experimental settings were arranged to run for 24, 36 or 48 hours. Such runs were done for the detector angles 90° and 180° .

After each run, data from the multichannel was printed on paper and punched on the paper tape. The single counts of γ_1 and γ_2 pulses obtained from the single channel analyser outputs were counted by using Philips timers (Model PW4260) and scalars (Model PW4230) and printed out every 10^3 secs. automatically. Also, the determination of time-zero was done after each set of runs at a given temperature.

Experiments were performed at -197°C , 0°C , room temperature i.e. 24°C , 200°C , 300°C . An experiment with powdered lead hafnate was also done at room

temperature.

The crystal was cooled to -197°C and 0°C by surrounding the crystal with liquid nitrogen and ice respectively. This was achieved by placing the crystal in a vacuum flask which was then filled with liquid nitrogen (for 197°C) and ice (for 0°C). The crystal was heated to the required temperature in a locally made heater. The temperature was monitored by means of a copper-constantan thermocouple and a digital multimeter.

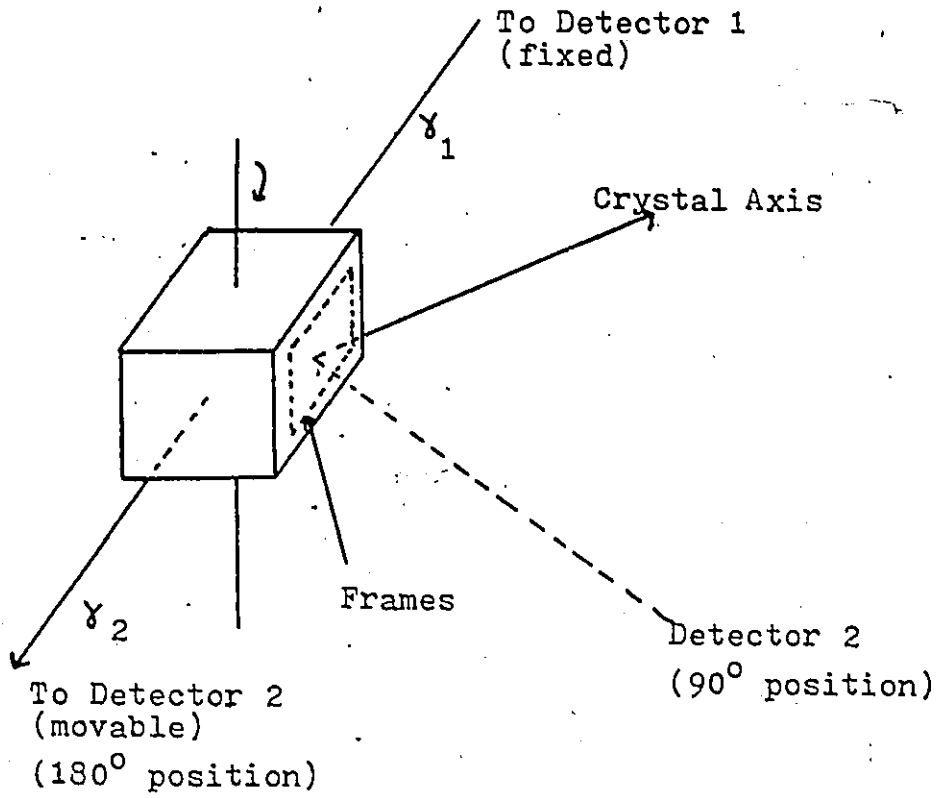


Fig. 3.5.1: Single Crystal PbHfO_3

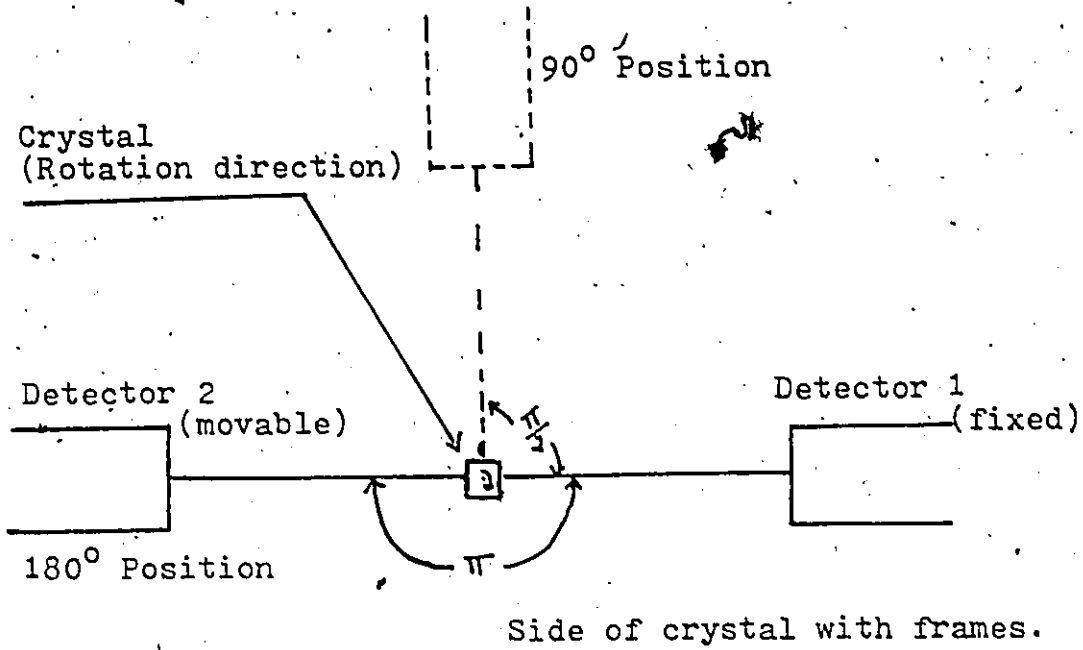


Fig. 3.5.2: Single Crystal PbHfO_3 and Detector Geometry

CHAPTER IV

RESULTS AND DISCUSSION

4.1 Results:

Experiments were carried out as follows: four runs using a polycrystalline source at room temperature, four runs using a single crystal at -197°C , 0°C , 24°C , 200°C and 300°C each. Also, each run consisted of two detector settings i.e. the 180° and 90° counter angles. The data collected at the end of each setting was used to compute the experimental anisotropy. This was done by feeding the tapes containing the information of the coincidence spectra remotely to the programmable calculator (Tetronix Model 31) through the tape reader on the teletype (Marsland, Model 811). These were connected by an interface (Tetronix Model 154). The tapes containing information of the single gamma counts were processed similarly.

For the analysis of the coincidence spectra, the calculator was programmed to carry out an exponential background subtraction. This was done for both detector settings. The calculator was also programmed to determine the mean values of the single gamma counts at both detector settings and to calculate the experimental anisotropy together with statistical errors. The time zero was found to be at the channel number 40.5. The single γ_1 and γ_2 rates also gave an indication of drift

in the energy spectrum. If the spectrum shifted and the window for γ_2 allows the 345 keV gamma-ray, the spectrum near time zero is distorted since it is in coincidence with the 136 keV gamma ray. Data showing significant drifts $> 5\%$ were rejected.

Thus, the experimental correlation $R(\theta)$ was found. This function corresponds to the theoretical perturbed correlation function $W(\theta)$ only under the assumption that we are dealing with centered point sources and point detectors. The crystal was small enough to be treated as a point source and the effect of the finite detector size is to reduce the value of $A_{22}G_{22}$ but not the variation with time. Therefore, no correction was made.

The calculated results are listed in the Tables II-VII.

Delay line no. (for every 2 rotations)	Centroid	Channels
2	10	0
4	15	5
6	20	5
8	25	5
10	30	5
12	35	5
14	40	5
16	45	5
18	50	5
20	55	5
22	60	5
24	65.74	5.74
26	71.0	5.26
	Mean	5.083

5.083 channels = 4.76 ns. = 2 rotations

1 channel = 0.936 ns.

TABLE I

POLYCRYSTALLINE SOURCE AT ROOM TEMPERATURE

Channel No.	Anisotropy	Error(±)
40	-.463	.039
41	-.316	.026
42	-.234	.018
43	-.181	.017
44	-.125	.019
45	-.088	.018
46	-.083	.024
47	-.005	.019
48	-.014	.018
49	-.034	.020
50	-.064	.032
51	-.012	.019
52	-.019	.018
53	-.093	.021
54	-.150	.027
55	-.143	.022
56	-.165	.025
57	-.241	.027
58	-.119	.024
59	-.114	.028
60	.017	.030
61	-.093	.027
62	-.103	.036
63	-.133	.037
64	-.102	.046
65	-.124	.031
66	-.094	.039
67	-.066	.044
68	-.140	.039
69	-.180	.046
70	-.155	.043
71	-.143	.040
72	-.126	.047
73	-.239	.055
74	-.195	.045
75	-.166	.076
76	-.053	.053
77	-.170	.052
78	-.295	.102
79	-.906	.110
80	-.184	.115
81	-.182	.102
82	-.148	.079
83	-.153	.083
84	-.021	.067
85	-.296	.151
86	.038	.090

TABLE II: RESULTS FOR FIG. (4.1.1)

SINGLE CRYSTAL AT -197°C

Channel No.	Anisotropy	Error(±)
40	.040	.031
41	.032	.025
42	-.042	-.023
43	.032	.022
44	.100	.023
45	.098	.023
46	.146	.024
47	.123	.026
48	.070	.026
49	-.019	-.028
50	-.057	-.029
51	-.076	-.030
52	-.150	-.031
53	-.143	-.032
54	-.064	-.033
55	.026	.035
56	.105	.035
57	.140	.037
58	.022	.038
59	.043	.040
60	.027	.041
61	.074	.043
62	0	-.044
63	-.055	-.047
64	-.092	-.049
65	-.160	-.052
66	-.081	-.051
67	.055	.055
68	-.107	-.057
69	.017	.06
70	.099	.066
71	.042	.065
72	.011	.069
73	0	.071
74	-.130	-.076
75	-.172	-.080
76	-.091	-.082
77	-.034	-.087
78	.124	.095
79	-.029	-.096
80	-.221	-.096
81	-.004	-.102
82	-.080	-.109
83	.037	.113
84	-.154	-.121
85	.026	.142
86	-.059	-.132

TABLE III: RESULTS FOR FIG. (4.1.2)

SINGLE CRYSTAL AT 0°C

Channel No.	Anisotropy.	Error(±)
40	-.195	.019
41	-.167	.017
42	-.161	.015
43	-.137	.015
44	-.087	.015
45	-.055	.018
46	-.106	.027
47	.004	.018
48	-.040	.020
49	-.059	.026
50	-.170	.023
51	-.145	.020
52	-.193	.019
53	-.173	.021
54	-.166	.021
55	-.218	.024
56	-.157	.022
57	-.127	.027
58	-.091	.025
59	-.103	.038
60	-.120	.027
61	-.096	.033
62	-.109	.033
63	-.108	.037
64	-.095	.040
65	-.077	.039
66	-.137	.036
67	-.187	.037
68	-.200	.041
69	-.150	.048
70	-.108	.048
71	-.104	.047
72	-.176	.071
73	-.245	.057
74	-.359	.070
75	-.289	.078
76	-.152	.050
77	-.147	.063
78	-.164	.070
79	-.195	.094
80	-.197	.072
81	-.400	.160
82	-.355	.120
83	-.169	.069
84	-.099	.079
85	-.225	.168
86	-.121	.106

TABLE IV : RESULTS FOR FIG. (4.1.3)

SINGLE CRYSTAL AT 24°C

Channel No.	Anisotropy	Error(\pm)
40	-.339	-.035
41	-.287	-.027
42	-.184	-.023
43	-.095	-.021
44	-.053	-.020
45	-.008	-.021
46	.029	.021
47	.068	.023
48	.077	.023
49	.051	.024
50	.002	.025
51	-.027	-.026
52	-.071	-.026
53	-.166	-.027
54	-.182	-.028
55	-.227	-.030
56	-.251	-.031
57	-.228	-.032
58	-.142	-.032
59	-.086	-.035
60	-.019	-.036
61	-.049	-.037
62	-.036	-.039
63	-.053	-.040
64	.108	.041
65	-.037	-.044
66	-.066	-.044
67	-.006	-.046
68	-.154	-.051
69	-.107	-.051
70	-.150	-.054
71	-.116	-.056
72	-.067	-.059
73	-.240	-.063
74	-.146	-.064
75	-.140	-.068
76	-.062	-.070
77	-.088	-.075
78	-.072	-.079
79	-.279	-.083
80	-.005	-.080
81	.013	.090
82	.013	.086
83	-.252	-.100
84	-.288	-.097
85	-.082	-.113
86	-.123	-.108

TABLE V: RESULTS FOR FIG.(4.14)

SINGLE CRYSTAL AT 200°C

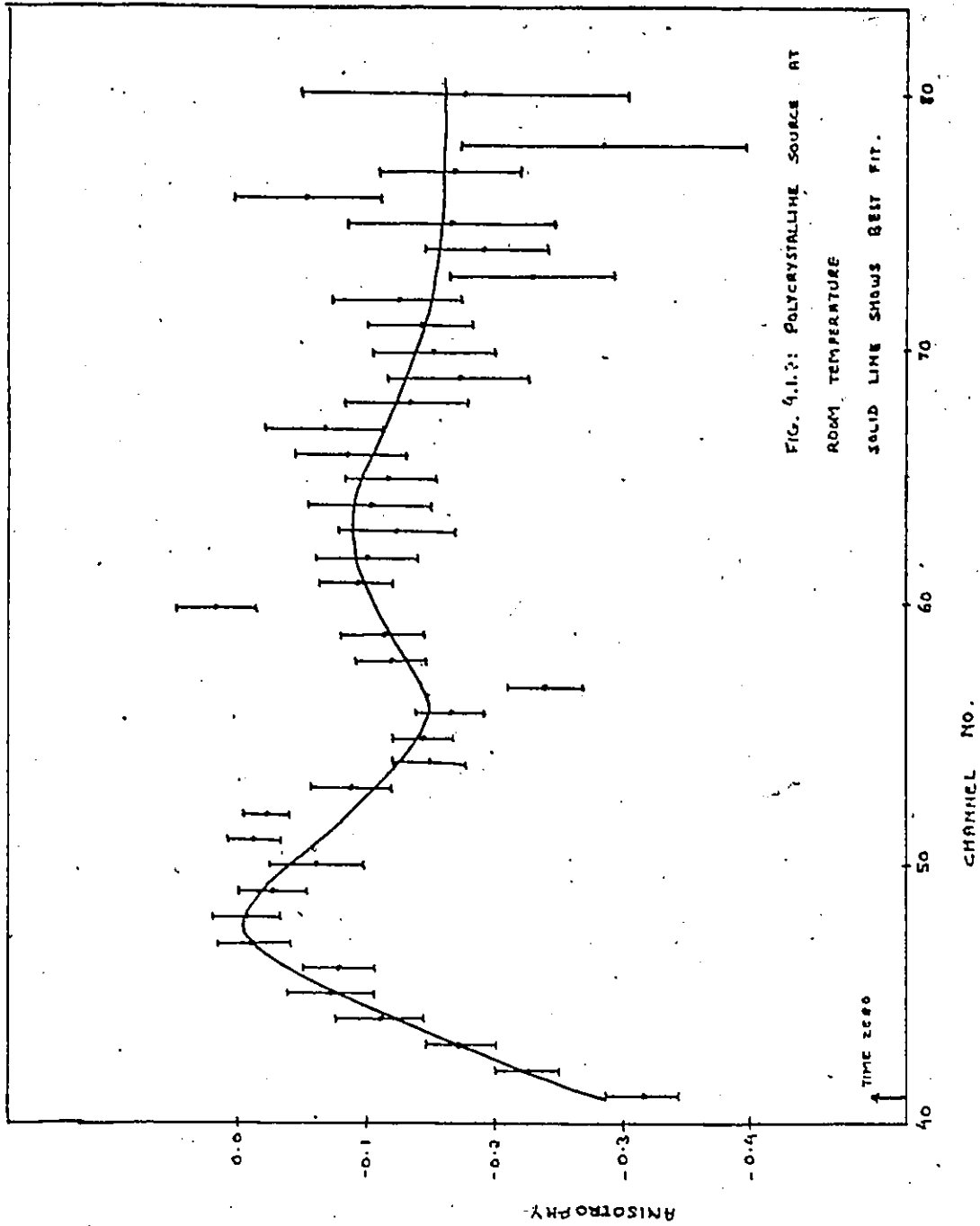
Channel No.	Anisotropy	Error(\pm)
40	-.242	-.078
41	-.235	-.052
42	-.184	-.037
43	-.189	-.030
44	-.212	-.027
45	-.239	-.027
46	-.249	-.027
47	-.189	-.028
48	-.218:	-.029
49	-.157	-.030
50	-.226	-.031
51	-.095	-.033
52	-.161	-.033
53	-.145	-.034
54	-.195	-.035
55	-.240	-.036
56	-.254	-.037
57	-.155	-.039
58	-.150	-.040
59	-.183	-.042
60	-.132	-.043
61	-.213	-.045
62	-.148	-.045
63	-.181	-.048
64	-.160	-.048
65	-.049	-.052
66	-.224	-.051
67	-.141	-.057
68	-.090	-.056
69	-.075	-.059
70	-.001	-.061
71	-.166	-.064
72	-.195	-.065
73	-.070	-.069
74	-.130	-.070
75	-.096	-.074
76	-.090	-.077
77	-.187	-.078
78	-.082	-.084
79	+.024	+.085
80	+.016	+.086
81	+.017	+.097
82	-.019	-.092
83	-.108	-.106
84	+.035	+.100
85	-.002	-.105

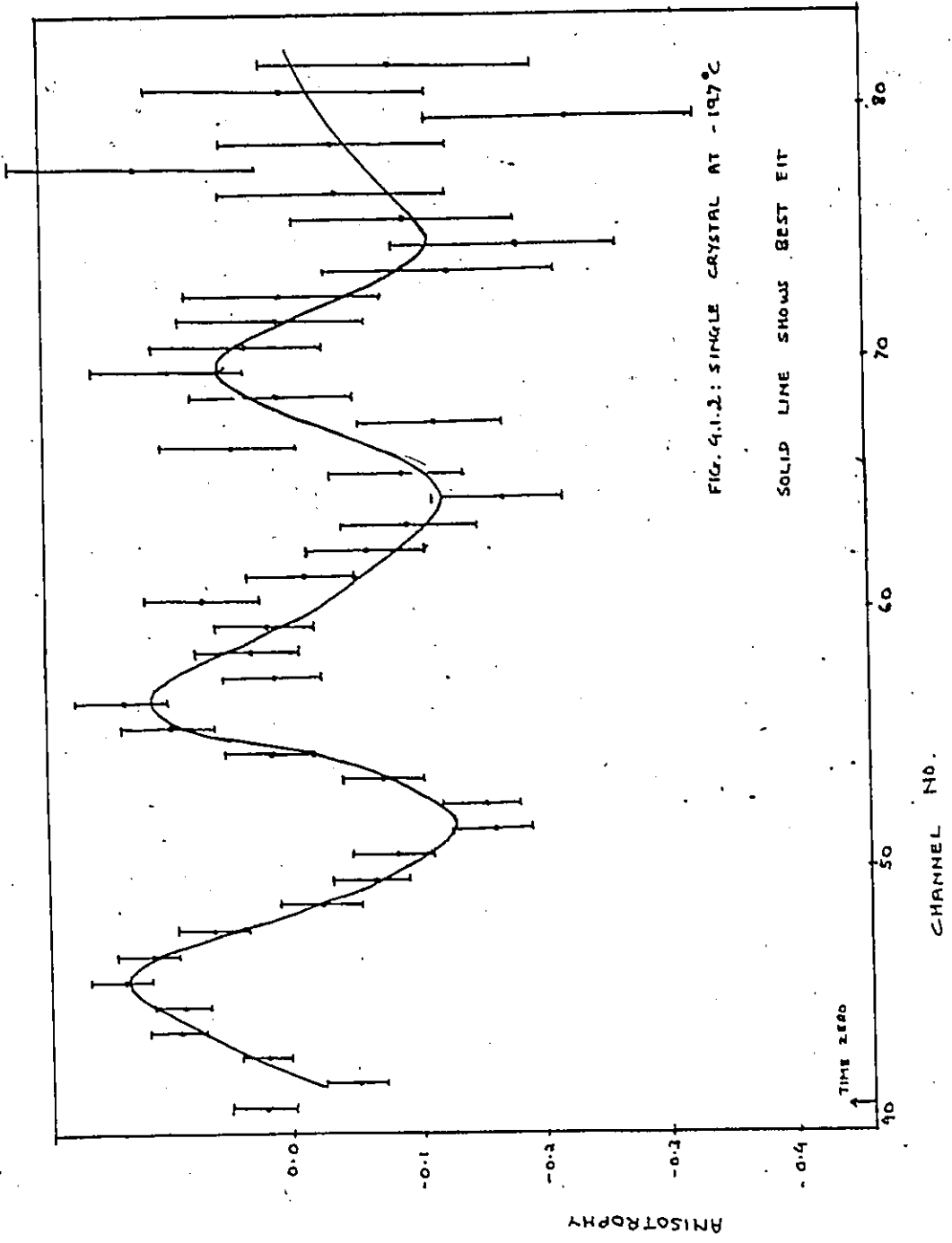
TABLE VI RESULTS FOR FIG.(4.1.5)

SINGLE CRYSTAL AT 300°C

Channel No.	Anisotropy	Error
40	-.286	-.068
41	-.335	-.047
42	-.345	-.036
43	-.292	-.032
44	-.230	-.031
45	-.296	-.032
46	-.278	-.033
47	-.296	-.034
48	-.328	-.034
49	-.313	-.036
50	-.312	-.037
51	-.249	-.038
52	-.294	-.040
53	-.272	-.041
54	-.288	-.041
55	-.272	-.044
56	-.180	-.044
57	-.333	-.047
58	-.270	-.047
59	-.293	-.051
60	-.234	-.052
61	-.286	-.055
62	-.228	-.055
63	-.307	-.058
64	-.322	-.057
65	-.288	-.062
66	-.334	-.064
67	-.305	-.066
68	-.219	-.070
69	-.289	-.071
70	-.378	-.072
71	-.272	-.076
72	-.277	-.080
73	-.333	-.083
74	-.339	-.085
75	-.362	-.090
76	-.093	-.088
77	-.004	-.100
78	-.303	-.093
79	-.271	-.106
80	-.489	-.107
81	-.342	-.124
82	-.403	-.115
83	-.241	-.119
84	-.080	-.137
85	-.491	-.134
86	-.503	-.143

TABLE VII: RESULTS FOR FIG.(4.1.6)





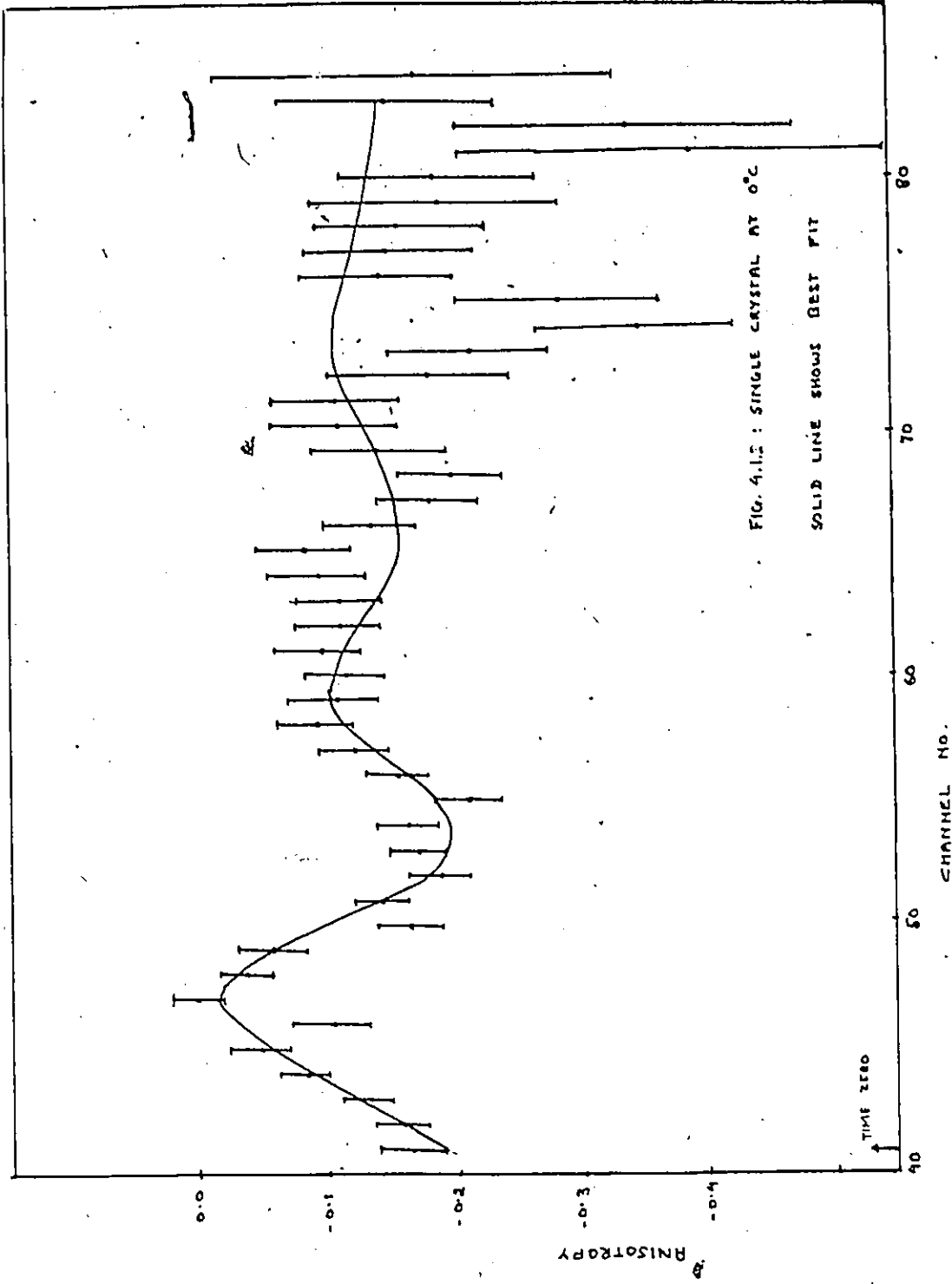
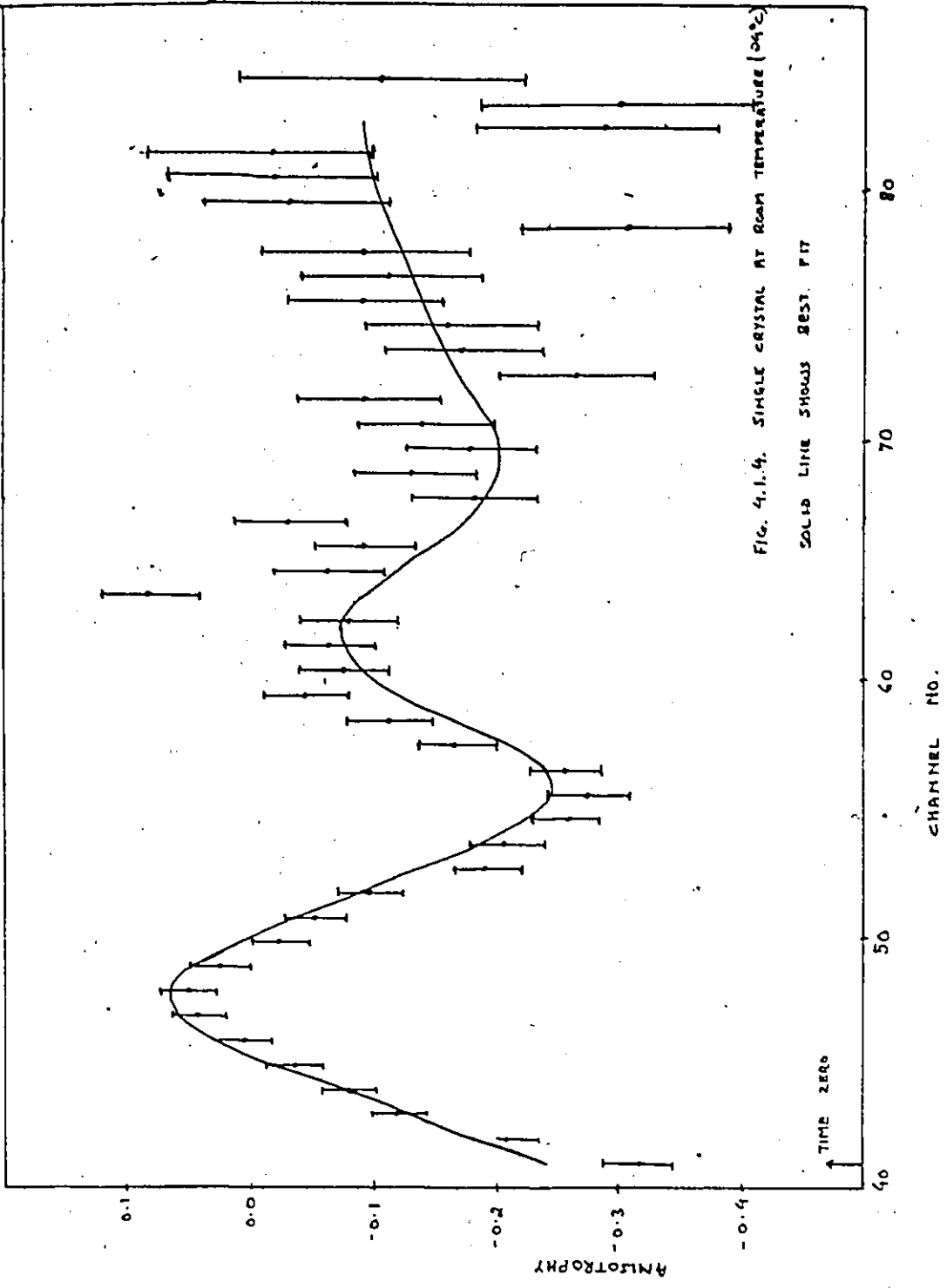
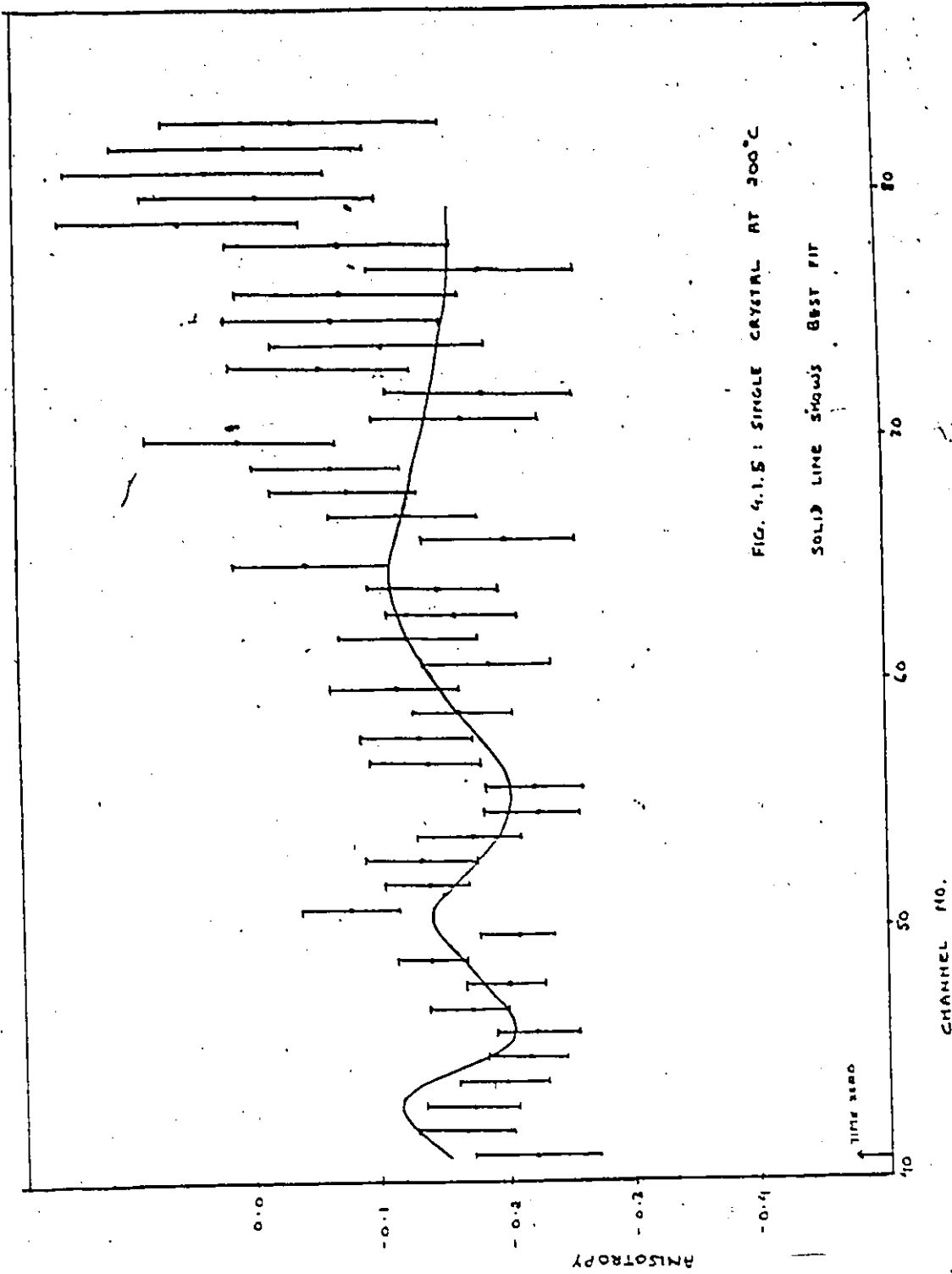
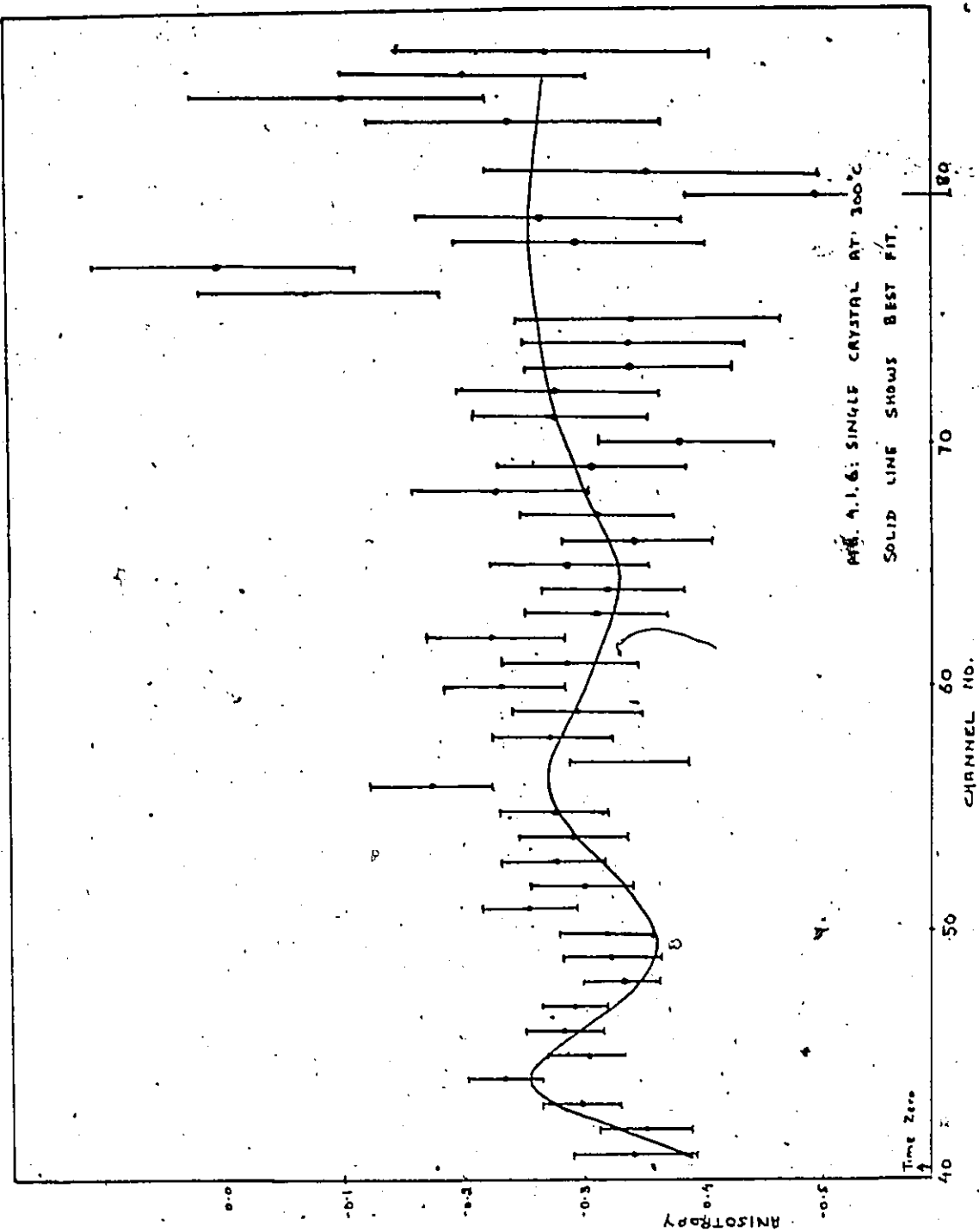


FIG. 4.1.2 : SINGLE CRYSTAL AT 0°C

SOLID LINE SHOWS BEST FIT







4.2 Discussion of Results:

Figs. (4.1.1) - (4.1.6) give the anisotropy versus time plots. It is observed that the correlation time spectra show damped oscillations. The reason attributed to this damping has been given as lattice imperfections and impurities. Hence, one would expect that at higher temperatures the damping will be more marked while it will be almost negligible at lower temperatures. This is verified, as seen from the figures.

Besides the damping of the oscillations, the time spectra for experiments conducted at higher temperatures show decrease in oscillatory pattern. This loss is attributed to the structural phase transformation of the perovskite antiferro-electric compound PbHfO_3 . According to Dernier et al (Mat. Res. Bull. 1975) the structure of lead hafnate has been found to transform from orthorhombic at room temperature through rhombohedral at about 180°C to cubic at about 250°C . The fact that a complete loss of oscillation could not be achieved shows that a small quadrupole interaction still exists. In the cubic phase ideally no quadrupole interaction should be present, but we are dealing with a real crystal with certain amount of lattice irregularities.

Such imperfections will destroy the cubic symmetry at some lattice sites and thus produce a small remaining interaction. Hence complete damping of oscillations does not occur. Another reason (M. Forker, 1972) could be as follows: since η is restricted by definition to the range $0 \leq \eta \leq 1$, a distribution of η can never have an average value of 0 or 1. Thus even in crystal phases e.g. cubic where the symmetry of the perfect crystal demands that $\eta = 0$, the time differential perturbation correlation measurements will give η values different from zero.

The fundamental frequency w_0 was determined from the Fourier power spectrum of the given perturbation function. This spectrum was calculated by numerical integration of the equation

$$P(w) = \left| \int_0^T A_{22} G_{22}(t) \exp(iwt) dt \right|^2$$

However, in this calculation T was taken as the life span over which statistically significant data was obtained and the value was approximately 36 nanoseconds. The power spectra of the perturbations are shown in Figs. (4.2.1) - (4.2.6). All curves were adjusted so that $P(0) = 0$. The values of w_0 obtained show that there is no evidence for the existence

of a second lattice site, since only one set of frequencies such that $w_1 + w_2 = w_3$ was seen.

The experimental anisotropy was compared with the one obtained by theoretical calculations, Eqn.(2.7.9) with A_k given by Eqn.(2.7.3). In this calculation symmetry about the z-axis was not assumed. The following parameters: the asymmetry η , w_0 , smearing δ , (a measure of the distribution of w_0 assuming a normal-shaped distribution), the Euler angles α and β (defined as in fig.4.2.7) and a delay parameter (used to shift the data in time since the $t = 0$ position did not necessarily coincide on the first channel position of the data under analysis) were varied until the best fit was obtained. The mixing ratios (Eqn. 2.7.8) and the time resolution of the system was also taken into account in the fitting process.

Using the best fits, the electric quadrupole frequency w_q and the maximal component of the quadrupole interaction V_{zz} were calculated. The EFG was calculated from the quadrupole frequency w_Q (defined in Eqn. 2,6.13) with the quadrupole moment as 2.53×10^{-28} barns. The variation of these quantities is shown in Table IX. The values of w_0 obtained seem to fit fairly well with those

obtained from the Fourier power spectrum.

Owing to lattice imperfections, it is frequently assumed that the EFG is not the same at all lattice sites, so that the frequencies are not sharply defined, but distributed with some relative width about a mean value (smearing δ). Hence, it would be expected that at lower temperatures δ is small, increasing with increase of temperature. This is confirmed as seen from Table IX. The value of η was seen to decrease with increase in temperature, but it did not vanish in the cubic phase for the reasons discussed before.

A quantitative analysis of the dependence of the quadrupole frequency w_Q on temperature was carried out. (Table X). It is observed that w_Q decreases with temperature as expected. (Forker et al. 1973).

The existence of a principal axis z' , different from the c-axis (z-axis) is shown in Fig. (4.2.7). This may be interpreted as arising from shifts of the Hf ions resulting in the deformed octahedral shapes about the Hf ions, as shown in Fig. (4.2.8). These shifts occur mainly in the x-y plane. The direction of the z' -axis is the direction of the EFG described by the Euler angles α and β . It is

seen that the value of β increases as the temperature increases indicating that the direction of the EFG is changing. The reason is the anisotropic expansion of the crystal i.e. as the temperature increases, the crystal goes through structural changes and therefore the lattice dimensions change, though not in a proportional manner. (Lead hafnate upto 163°C is tetragonal with $c/a < 1$, and above this, in the range $163^{\circ} - 215^{\circ}\text{C}$ it is still tetragonal with c/a larger than before but still less than unity.

Thus, we can conclude that the technique of the perturbed angular correlations is suitable for the study of properties of antiferro-electric compounds.

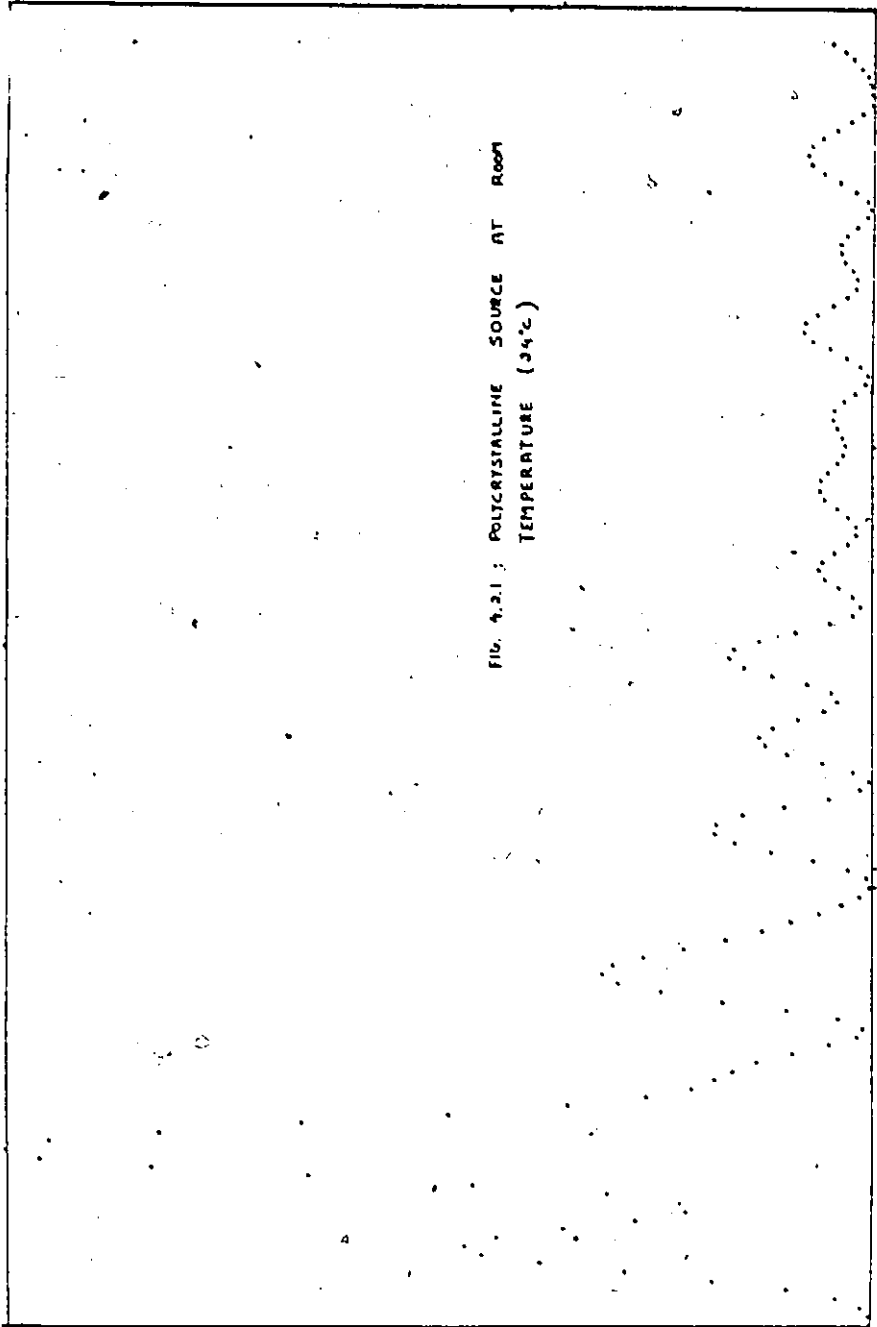


FIG. 4.2.1: POLYCRYSTALLINE SOURCE AT ROOM TEMPERATURE (34°C)

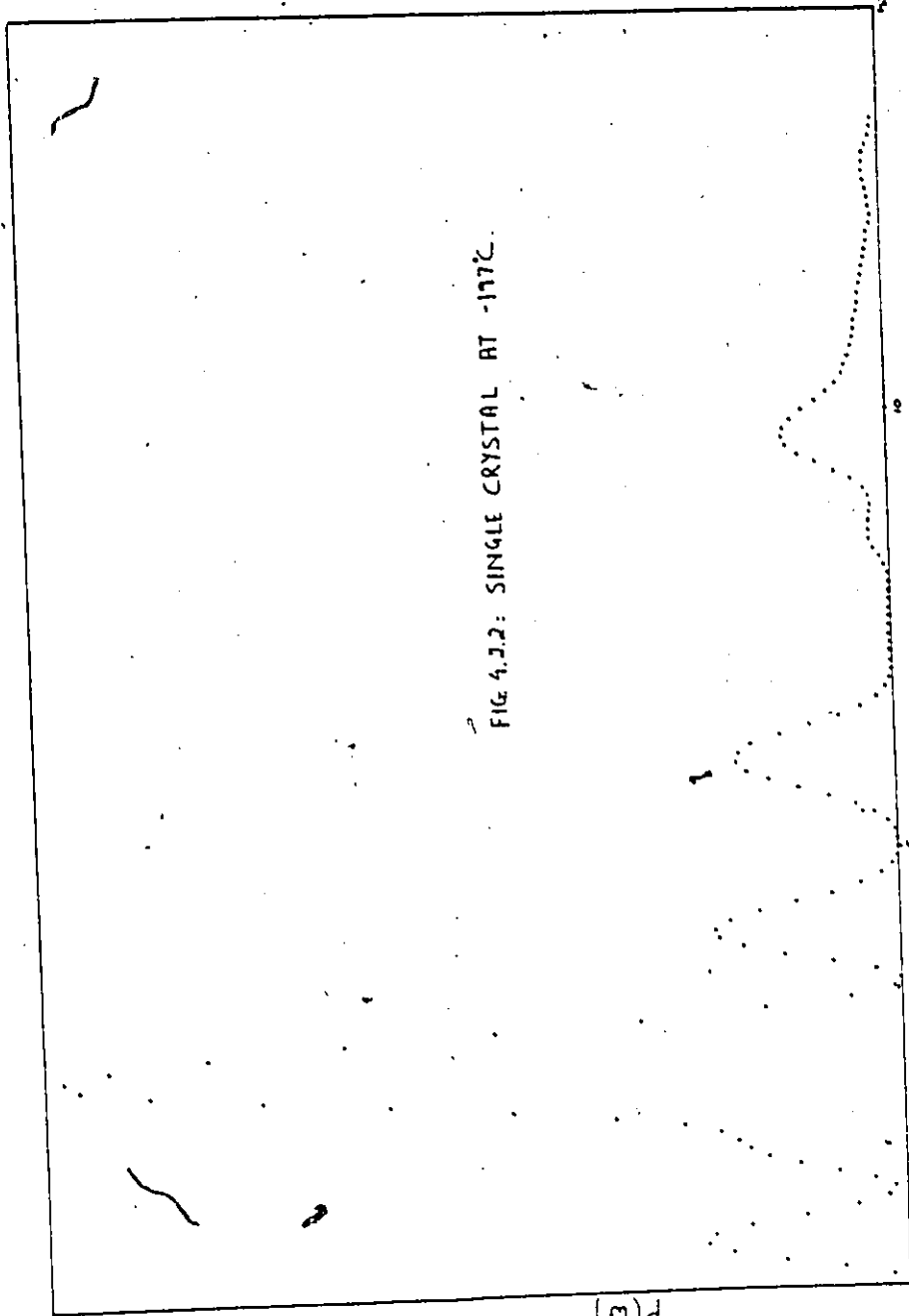


FIG 4.3.2: SINGLE CRYSTAL AT -197°C

(10⁻⁴) RAD/NS

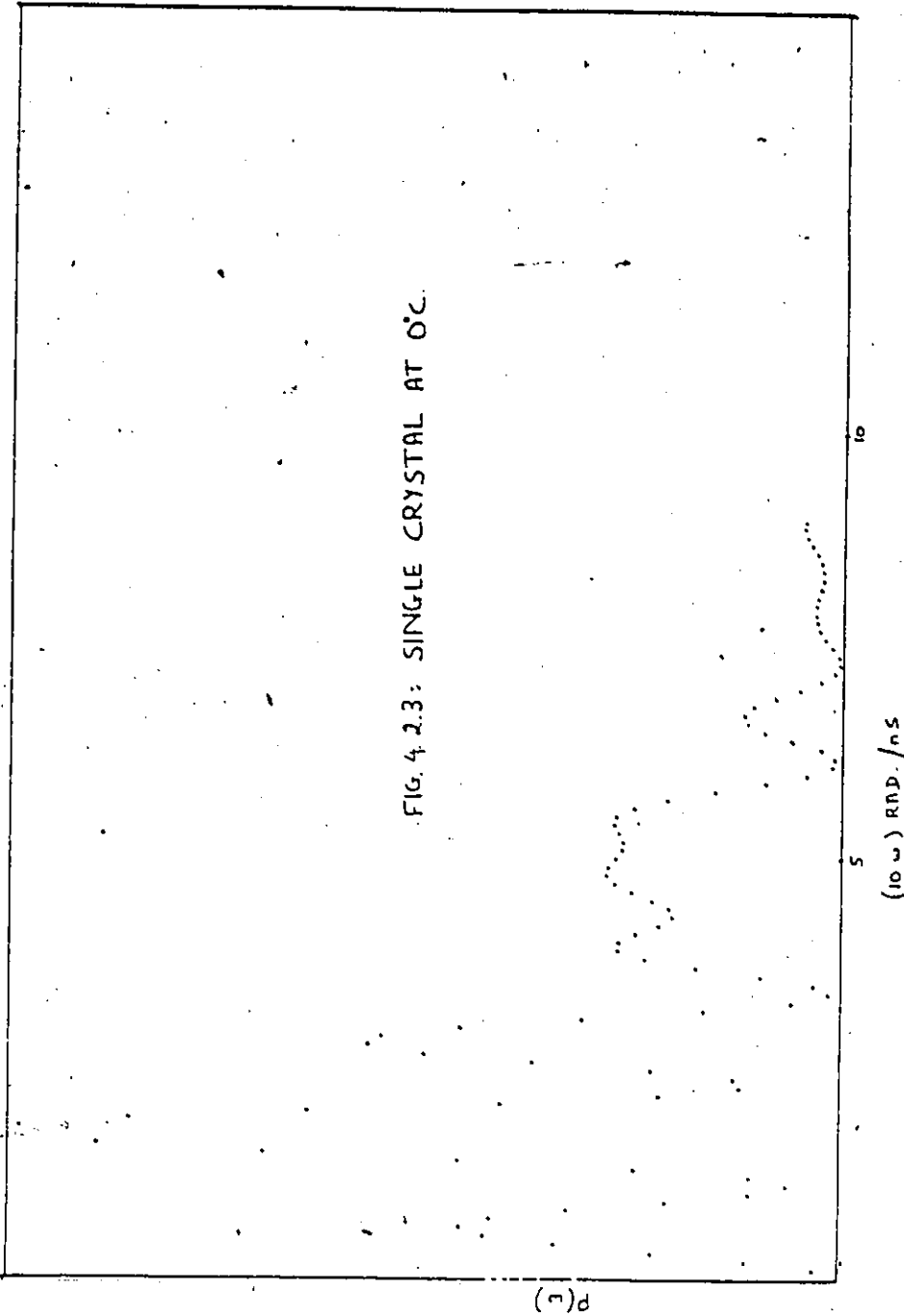
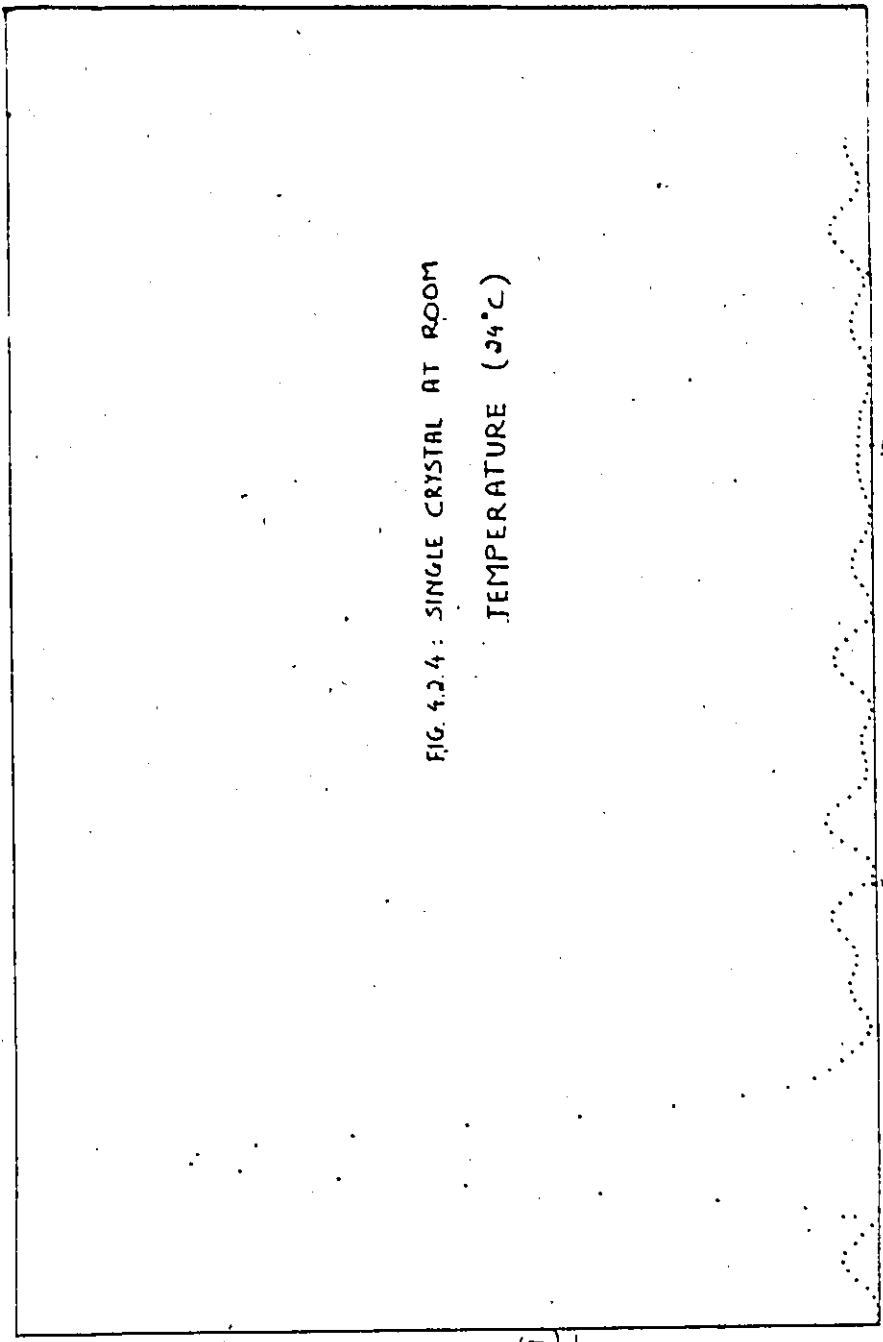


FIG. 4.2.4: SINGLE CRYSTAL AT ROOM
TEMPERATURE (24°C)



(10 ω) RAD/NS

$P(\omega)$

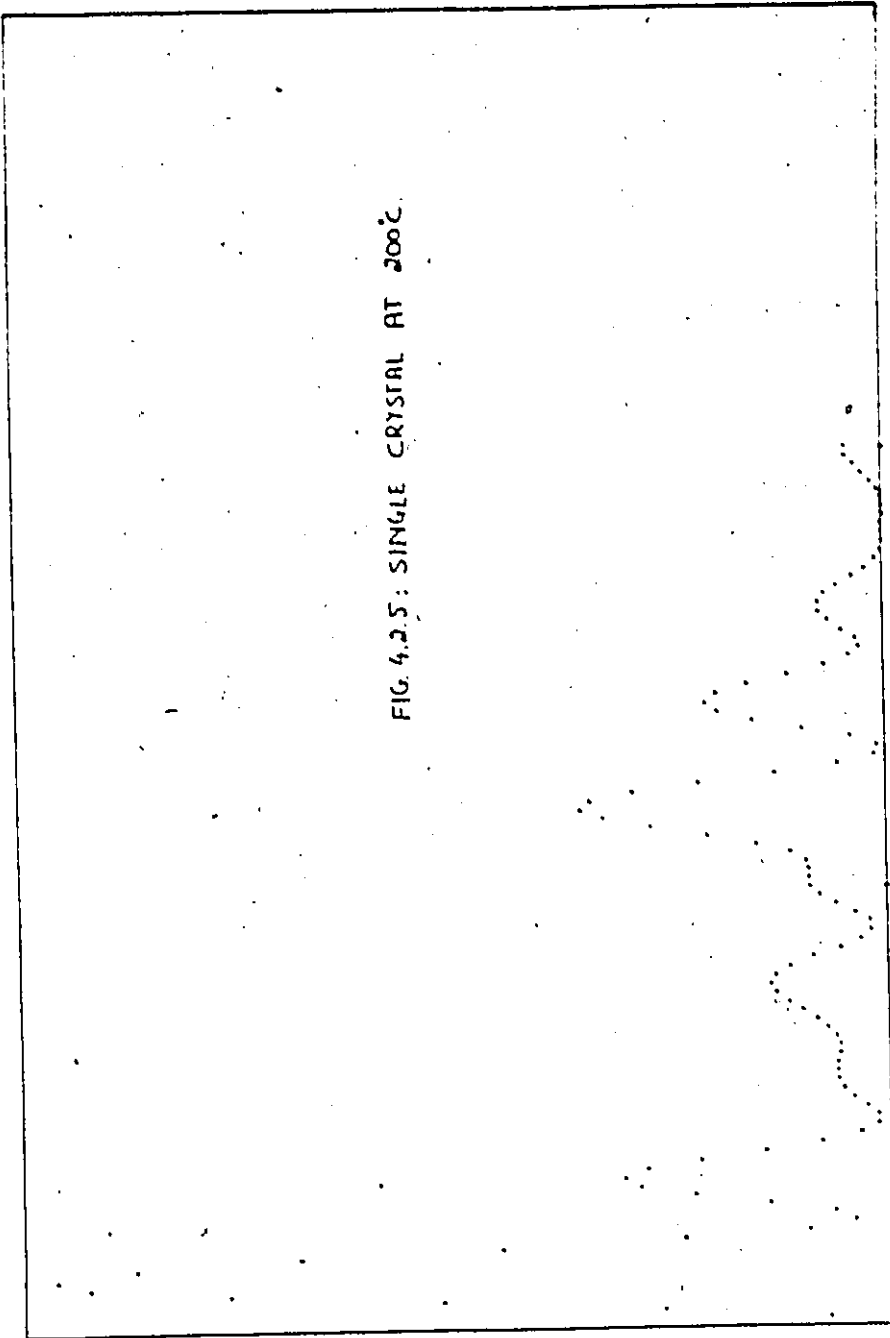


FIG. 4.2.5: SINGLE CRYSTAL AT 200°C.

$P(\omega)$

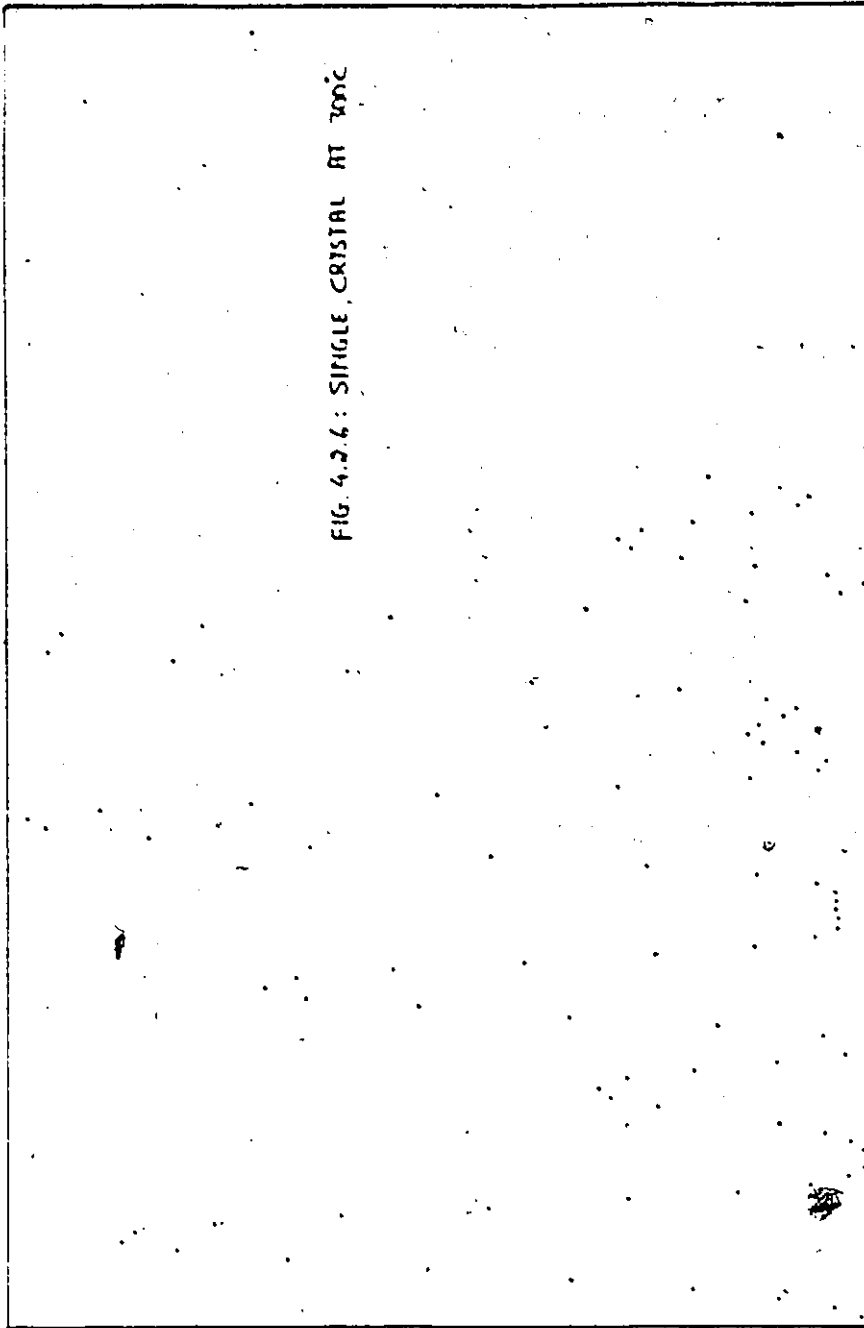


FIG. 4.2.6: SINGLE CRYSTAL AT 300°C

(10 ω) RND / NS

(n)d

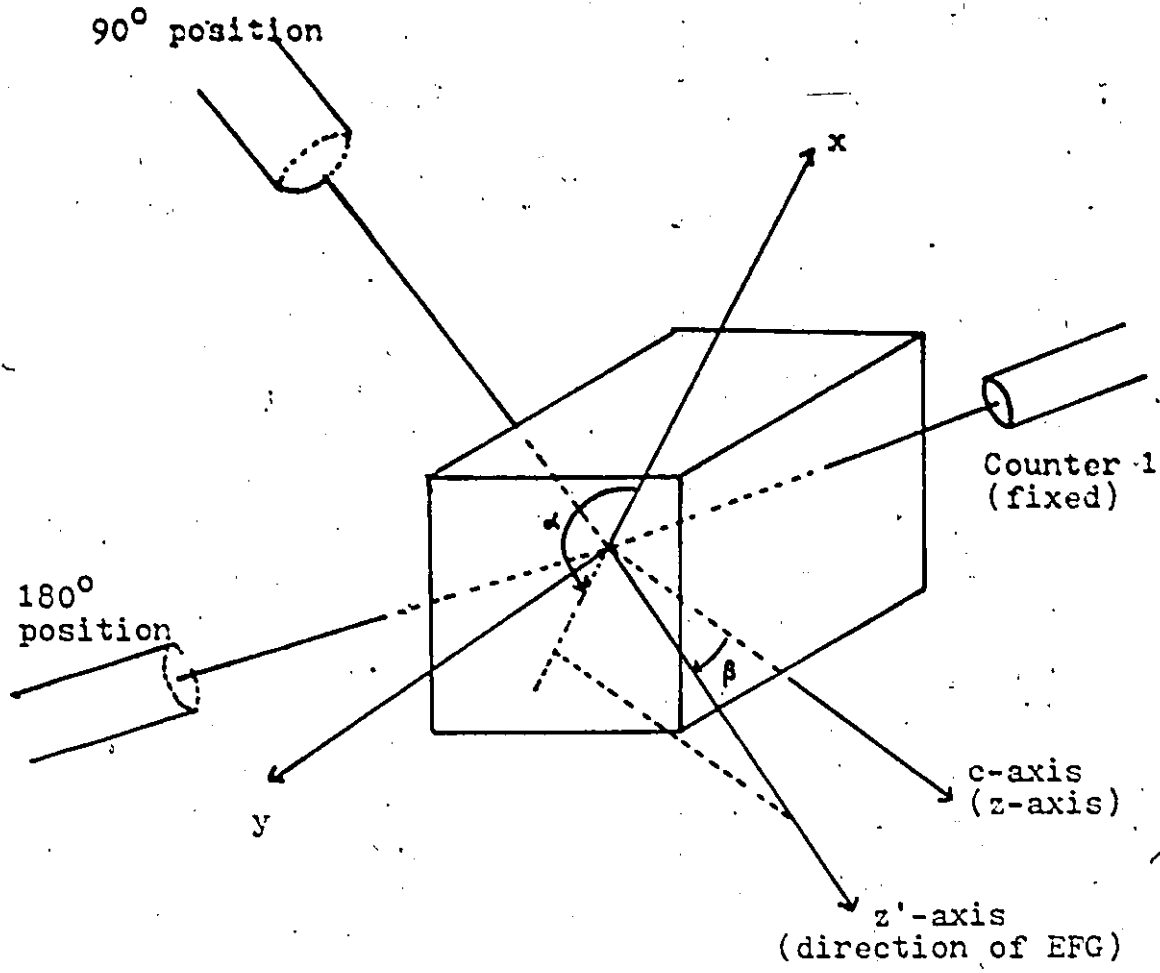
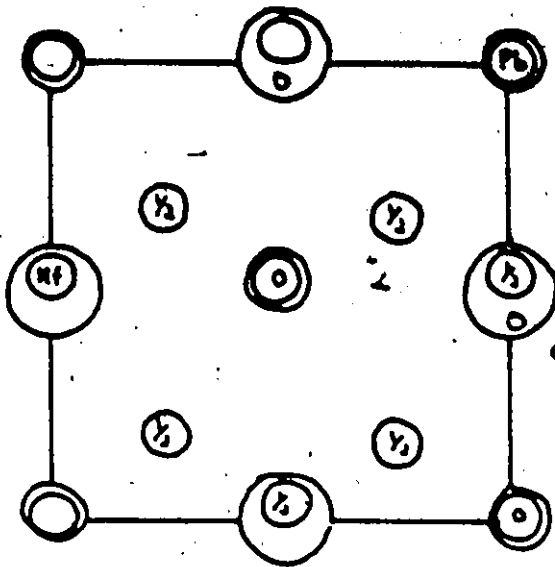
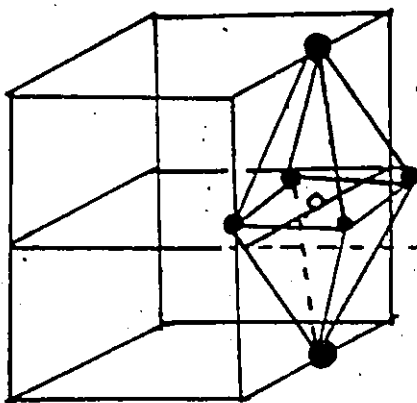


Fig. 4.2.7: Geometry of the Apparatus showing Euler angles.



(A) A projection along a_1 axis of the orthorhombic low temperature modification of lead hafnate. (Origin is at the lower right).



(B) Structure around Hf ions giving rise to crystalline field.

Fig. 4.2.8: $PbHfO_3$ crystalline structure.

	$w_0 z$	η	$\delta\%$
Value	3.85	0.22	23.5
Error (\pm)	0.05	0.05	5%

TABLE VIII: Values of various parameters for the polycrystalline source

$$\Delta_{482} = -0.137$$

$$\Delta_{137} = -2.22$$

Temperature	$w_0 z$	η	δ	α	β
-197°C	3.36 ± 0.05	0.54 ± 0.05	6.00%	0.055	0.24
0°C	3.15 ± 0.05	0.50 ± 0.05	10.0%	0.055	0.27
24°C	2.94 ± 0.05	0.46 ± 0.05	12.5%	0.055	0.30
200°C	1.35 ± 0.05	0.29 ± 0.05	25.4%	0.055	0.33
300°C	1.14 ± 0.05	0.18 ± 0.05	24.8%	0.055	0.40

TABLE IX: Single Crystal source - Variation of parameters with temperature.

$$\Delta_{482} = -0.137$$

$$\Delta_{137} = -2.22$$

Temperature	Quadrupole frequency w_Q (MHz)	$ V_{zz} $ (V/cm ²)
-197°C	51.85 ± 0.77	$5.39 \pm 0.07 \times 10^{17}$
0°C	48.62 ± 0.77	$5.05 \pm 0.07 \times 10^{17}$
24°C	45.36 ± 0.77	$4.71 \pm 0.07 \times 10^{17}$
200°C	20.75 ± 0.77	$2.16 \pm 0.07 \times 10^{17}$
300°C	17.62	$1.83 \pm 0.07 \times 10^{17}$

TABLE X: Variation of w_Q and $|V_{zz}|$ with temperature.

APPENDIX

A.I Vector Addition Coefficients and Racah Algebra:

Consider a system consisting of two non-interacting parts, each of which is characterised by its total angular momentum and a component in some specified direction. Let j_1 , j_2 and j denote the angular momenta and m_1 , m_2 and m correspond to their associated magnetic quantum numbers respectively. The Clebsch-Gordan coefficients for the vector addition $j_1 + j_2 = j$, $m_1 + m_2 = m$ are defined by the transformation:

$$|j_1 j_2 j m\rangle = \sum_{m_1, m_2} \langle j_1 j_2 m_1 m_2 | j m \rangle |j_1 m_1\rangle |j_2 m_2\rangle \quad (A.1)$$

These coefficients are the elements of a unitary matrix and the phases of the eigen-functions are chosen such that the C-G coefficients are real numbers and hence the matrix is orthogonal.

Calculations become simpler if the C-G coefficients are replaced by the more symmetric Wigner 3-j symbols. These symbols are related to the C-G coefficients by:

$$\begin{pmatrix} j_1 & j_2 & j \\ m_1 & m_2 & m \end{pmatrix} = (-1)^{j_1 - j_2 - m} (2j+1)^{-\frac{1}{2}} \langle j_1 m_1 j_2 m_2 | j -m \rangle \quad (A.2)$$

These 3-j symbols possess simple symmetry properties.

An even permutation of the columns leaves the coefficient unchanged while an odd permutation or an interchange of all m to $-m$ is equivalent to a multiplication by $(-1)^{j_1+j_2+j}$

$$\begin{pmatrix} j_1 & j_2 & j \\ m_1 & m_2 & m \end{pmatrix} = \begin{pmatrix} j_2 & j & j_1 \\ m_2 & m & m_1 \end{pmatrix} = \begin{pmatrix} j & j_1 & j_2 \\ m & m_1 & m_2 \end{pmatrix} \quad (\text{A.3})$$

$$\begin{pmatrix} j_1 & j_2 & j \\ m_1 & m_2 & m \end{pmatrix} = (-1)^{j_1+j_2+j} \begin{pmatrix} j_2 & j_1 & j \\ m_2 & m_1 & m \end{pmatrix} \quad (\text{A.4})$$

The 3-j symbols satisfy the following orthogonality relations:

$$\sum_{j,m} (2j+1) \begin{pmatrix} j_1 & j_2 & j \\ m_1 & m_2 & m \end{pmatrix} \begin{pmatrix} j_1 & j_2 & j \\ m'_1 & m'_2 & m \end{pmatrix} = \delta_{m_1 m'_1} \delta_{m_2 m'_2} \quad (\text{A.5})$$

$$\sum_{m_1, m_2} (2j+1) \begin{pmatrix} j_1 & j_2 & j \\ m_1 & m_2 & m \end{pmatrix} \begin{pmatrix} j_1 & j_2 & j' \\ m_1 & m_2 & m' \end{pmatrix} = \delta_{jj'} \delta_{mm'} \quad (\text{A.6})$$

In the calculation of the correlation function, sums over products of 3-j symbols appear. Such sums can be performed by using the Wigner 6-j symbol or the related Racah coefficient.

Consider a system made up of three distinct systems 1, 2 and 3 with angular momentum j_1 , j_2 and j_3 respectively.

The total angular momentum is then

$$J = j_1 + j_2 + j_3$$

The addition problem consists in forming the eigenvectors of the total angular momentum in the space spanned by the $(2j_1+1)$, $(2j_2+1)$ and $(2j_3+1)$ eigenvectors

$$|j_1 j_2 j_3 m_1 m_2 m_3\rangle$$

of individual angular momenta corresponding to well-defined values of the quantum numbers j_1 , j_2 and j_3 . There are several ways of constructing the vectors of angular momentum (JM):

- (i) j_1 and j_2 can be coupled to form the angular momentum $J_{12} = j_1 + j_2$ and then J_{12} and j_3 can be coupled to form J . In this way the eigenvectors obtained are

$$|(j_1 j_2)_{J_{12}}, j_3; JM\rangle = \sum_{\substack{m_1, m_2 \\ M_{12}, m_3}} |j_1 j_2 j_3 m_1 m_2 m_3\rangle \\ \times \langle j_1 j_2 m_1 m_2 | J_{12} M_{12} \rangle \langle J_{12} j_3 M_{12} m_3 | JM \rangle$$

(A.7)

common to $j_1^2, j_2^2, j_3^2, J_{12}^2, J^2$ and J_z .

(ii) j_2 and j_3 can be coupled to form the angular momentum $J_{23} = j_2 + j_3$ and then j_1 and J_{23} can be coupled to form J . The eigenfunctions obtained are:

$$|j_1(j_2j_3)J_{23}, JM\rangle = \sum_{\substack{m_2, m_3 \\ m_1, M_{23}}} |j_1j_2j_3, m_1m_2m_3\rangle \\ \times \langle j_2j_3, m_2m_3 | J_{23} M_{23} \rangle \langle j_1J_{23}, m_1M_{23} | JM \rangle. \quad (\text{A.8})$$

common to $j_1^2, j_2^2, j_3^2, J_{23}^2, J^2$ and J_z .

(iii) j_1 and j_3 can be coupled to form J_{13} and J_{13} and j_2 coupled to form J .

Thus, there is a choice between three different sets of basis vectors for the total angular momentum. In many problems it is useful to be able to pass from one set to another. The transformation involved is a unitary transformation, e.g.

$$|j_1(j_2j_3)J_{23}; JM\rangle = \sum_{J_{12}} |(j_1j_2)J_{12}j_3; JM\rangle \\ \times \langle (j_1j_2)J_{12}j_3^J | j_1(j_2j_3)J_{23}^J \rangle \quad (\text{A.9})$$

The coefficients of this unitary transformation are independent of M as can be seen by applying J_+ or J_- to both sides of the equation above. They depend only on the six angular momenta $j_1, j_2, j_3, J_{12}, J_{23}$ and J .

Rather than use these coefficients it is more convenient to use the Racah W coefficient, defined as follows:

$$\begin{aligned} \langle (j_1 j_2)_{J_{12}}, j_3^J | j_1 (j_2 j_3)_{J_{23}}^J \rangle &= \sqrt{(2J_{12}+1)(2J_{23}+1)} \\ &\quad W(j_1 j_2 j_3; J_{12} J_{23}) \\ &= (-)^{j_1+j_2+j_3+J} \sqrt{(2J_{12}+1)(2J_{23}+1)} \begin{Bmatrix} j_1 & j_2 & J_{12} \\ j_3 & J & J_{23} \end{Bmatrix} \quad (\text{A.10}) \end{aligned}$$

It is clear from this definition, that the W coefficients are simply the sum over the 'm' indices of four C-G coefficients.

A.II Rotational Matrices.

The transformation properties of eigenfunctions of angular momentum under the rotation of the co-ordinate axis are also needed. The rotations taking one co-ordinate system into another are specified by the Euler angles (θ, ϕ, ψ) .

Corresponding to a rotation operator $D(\alpha \beta \gamma)$ there is a rotation matrix $D^J(\alpha \beta \gamma)$ which is $(2J+1)$ dimensional. By definition:

$$D_{MM'}^J(\alpha \beta \gamma) = \langle JM | D(\alpha \beta \gamma) | JM' \rangle \quad (\text{A.11})$$

These matrices constitute a convenient representation of the operators $R(\alpha \beta \gamma)$ and are commonly used each time it is necessary to change the orientation of the state vector or observables.

These matrices have the following properties:

(i) Product of two matrices corresponding to the rotation R_1 and R_2 is the matrix corresponding to the rotation $R_1 R_2$:

$$D_{MM'}^J(R_1 R_2) = \sum_{M''} D_{MM''}^J(R_1) D_{M''M'}^J(R_2) \quad (\text{A.13})$$

(ii) The matrices associated with R and R^{-1} are

$$D_{MM'}^J(R) = D_{M'M}^J(R^{-1})^* \quad (\text{A.14a})$$

where $R^{-1} = (-\psi, -\phi, -\theta)$ if $R = (\theta, \phi, \psi)$

(iii) Symmetry relations:

$$D_{MM'}^{(J)*} = (-)^{M-M'} D_{-M, -M'}^{(J)} \quad (A.14b)$$

(iv) The product of two matrix elements of the rotation group can be expressed as a sum over matrix elements (C-G series)

$$D_{MM'}^J D_{M'M}^{J'} = \sum_{kZN} \langle J \uparrow J' \uparrow \uparrow | k z \rangle \langle J M J' M' | k N \rangle D_{ZN}^k \quad (A.15)$$

The summation index runs from $|J-J'|$ to $|J+J'|$
 $N = M + M'$; $Z = \uparrow + \uparrow'$

$$(v) D_{M0}^J(\theta, \phi, \psi) = \sqrt{\frac{4\pi}{2J+1}} Y_J^{M*}(\phi, \theta) \quad (A.16)$$

$$D_{0M}^J(\theta, \phi, \psi) = \sqrt{\frac{4\pi}{2J+1}} Y_J^{-M}(\phi, \psi) \quad (A.17)$$

$$D_{00}^J(\theta, \phi, \psi) = P_J(\cos \phi) \quad (A.18)$$

where $Y_J^M, Y_J^{M'}$ are spherical harmonics

$P_J(\cos \phi)$ are Legendre's polynomials.

A.III Density Matrices:

Assume that the eigenstates of a certain operator form a complete orthonormal set $|m\rangle$. Assume that the system under discussion be in a pure state $|n\rangle$. This state $|n\rangle$ can be expanded in terms of the states $|m\rangle$

$$|n\rangle = \sum_m a_{nm} |m\rangle \quad (A.19)$$

The expectation value of an operator F in the state $|n\rangle$ is given by

$$\langle n|F|n\rangle = \sum_{m',m} a_{nm'}^* a_{nm} \langle m'|F|m\rangle \quad (A.20)$$

If the system is in a mixed state, it cannot be described by a single state $|n\rangle$. Instead, it must be given as an incoherent sum of pure states $|n\rangle$ with weights g_n . The expectation value F of the ensemble becomes

$$\langle F \rangle = \sum_n g_n \langle n|F|n\rangle = \sum_{nm'm} g_n a_{nm'}^* a_{nm} \langle m'|F|m\rangle \quad (A.21)$$

Defining the matrix elements of a density operator ρ by

$$\langle m|\rho|m'\rangle = \sum_n g_n a_{nm'}^* a_{nm} \quad (A.22)$$

gives

$$\langle F \rangle = \sum_{mm'} \langle m|\rho|m'\rangle \langle m'|F|m\rangle \quad (A.23)$$

$$\text{or } \langle F \rangle = \text{Tr}(\rho F) = \text{Tr}(F \rho) \quad (\text{A.24})$$

Tr denotes trace or sum of diagonal elements of the matrix \hat{F} , while $\langle m | \rho | m' \rangle$ is called the density matrix.

Four useful applications of the density matrix formalism are:

- (1) Assume that $2I+1$ states $|n\rangle$ exist and that all have equal weight and are equally populated. The states $|m\rangle$ can be selected such that the density matrix is diagonal

$$\langle m' | \rho | m \rangle = (2I+1)^{-1} \delta_{mm'} \quad (\text{A.25})$$

- (2) The probability of finding the pure state $|n\rangle$ in the state $|m\rangle$ is given by $a_{nm}^* a_{nm}$. The probability $P(m)$ of finding in the state $|m\rangle$ any member of a mixed ensemble described by the incoherent superposition of states $|n\rangle$ is given

$$\text{by } \sum_n g_n a_{nm}^* a_{nm}, \quad \text{or}$$

$$P(m) = \langle m | \rho | m \rangle \quad (\text{A.26})$$

The diagonal elements of the density matrix give the probability $P(m)$ of finding the ensemble in state $|m\rangle$.

- (3) Considering transitions from a certain level A to a level B we shall denote the set of quantum

numbers describing eigenstates of level A by

a, a' ... and states of level B by b, b'...

The operator H inducing transitions from A to B

is assumed to linear but not necessarily

Hermetian

$$\langle f|H|i\rangle^* = \langle i|H^\dagger|f\rangle \quad (\text{A.27})$$

Assuming that the system is initially in an

eigenstate $|a\rangle$ of level A, the transition results

in a state

$$|f\rangle = H|i\rangle \quad \langle f| = \langle i|H^\dagger \quad (\text{A.28})$$

that is not necessarily an eigenstate of B.

The probability $P_B(b)$ of finding the system after transition in a certain eigenstate $|b\rangle$ is given by:

$$P_B(b) = |\langle b|f\rangle|^2 = |\langle b|H|a\rangle|^2 \quad (\text{A.29})$$

(4) Generally, the system is not initially in an eigenstate, but will be described by a density operator

$$\rho_A = \sum_n |n\rangle g_n \langle n|$$

After the transition induced by the operator H, the density operator in the level B will be

$$\rho_B = \sum_n H|n\rangle g_n \langle n|H^\dagger$$

since each state $|n\rangle$ changes according to Eqn. (A.28)

Taking matrix elements gives

$$\langle b | \rho_B | b' \rangle = \sum_n \langle b | H | n \rangle g_n \langle n | H^\dagger | b' \rangle \quad (\text{A.30})$$

In terms of the eigenstates $|a\rangle$ we get

$$\begin{aligned} \langle b | \rho_B | b' \rangle &= \sum_{aa'n} \langle b | H | a \rangle \langle a | n \rangle g_n \langle n | a' \rangle \langle a' | H | b' \rangle \\ &= \sum_{aa'} \langle b | H | a \rangle \langle a | \rho_A | a' \rangle \langle b' | H | a' \rangle^* \quad (\text{A.31}) \end{aligned}$$

A.IV Wigner-Eckart Theorem:

The matrix element of a tensor operator T_q^λ of a tensor of rank λ can be written as a product of a 3-j symbol (geometrical factor) and a scalar factor, the reduced matrix element which does not depend on any magnetic quantum number

$$\langle I m | T_q^\lambda | I_i m_i \rangle = (-1)^{I-m} \begin{pmatrix} I & \lambda & I_i \\ -m & q & m_i \end{pmatrix} \langle I || T^\lambda || I_i \rangle \quad (A.32)$$



BIBLIOGRAPHY

1. Alder, K et al., *Helv. Phys. Acta*, n26, pp 761-783 (1953)
2. Brink, D.M. and Satchler, G.R., "Angular Momentum", Oxford University Press (1971)
3. Dernier, P.D. et al., *Mat. Res. Bull.* 10, 187 (1975)
4. Forker, M et al., *Physical Review B*, v7, n3, pp1039-1047 (1973)
5. Forker, M and Hammersfahr, A., *Z Physik*, v255, pp 196-205 (1972)
6. Frauenfelder, H., *Annual Review of Nuclear Science*, v2, pp 129-153 (1953)
7. Kittel, C., "Solid State Physics", J.Wiley & Sons, New York (1953)
8. Kowalski, E., "Nuclear Electronics", Springer-Verlag, (1970)
9. Messiah, A., "Quantum Mechanics", J.Wiley & Sons, New York (1962)
10. Seigbahn, K., "Alpha, Beta and Gamma-Ray Spectroscopy" Chapter XIX by Frauenfelder, H and Steffen, R.M., North Holland Publishing Company, Amsterdam, (1965)
11. Vianden, R.J. & Kaufmann, E.N., *Rev. Mod. Phys.* v51 p163 (1979)
12. Yates, M.J.L., "Perturbed Angular Correlations" by Karlson, E, Matthias, E and Seigbahn, K., North Holland Publishing Company, (1963)
13. Ling, D.S. & Falkoff, D.L., *Phys. Rev.* 76, 1639 (1949)

VITA AUCTORIS

Place of Birth: India

Date: March 14, 1957.

Education: 1971 Indian School Certificate

1974 Bachelor of Science (Physics,
Chemistry and Mathematics)
University of Lucknow, Lucknow, India

1975 B.Sc. Hons. (Physics)
University of Lucknow, Lucknow, India.

1976 Master of Science (Special) in Physics
University of Lucknow, Lucknow, India.

1977 Research Fellow (Astrophysics)
U.P. State Observatory, India.

1978 Entered Graduate School, University
of Windsor.

Awards: 1975 University of Lucknow Scholarship.

1976 University of Lucknow Scholarship.

1978 University of Windsor Post-Graduate
Scholarship.

1979 University of Windsor Post-Graduate
Scholarship.